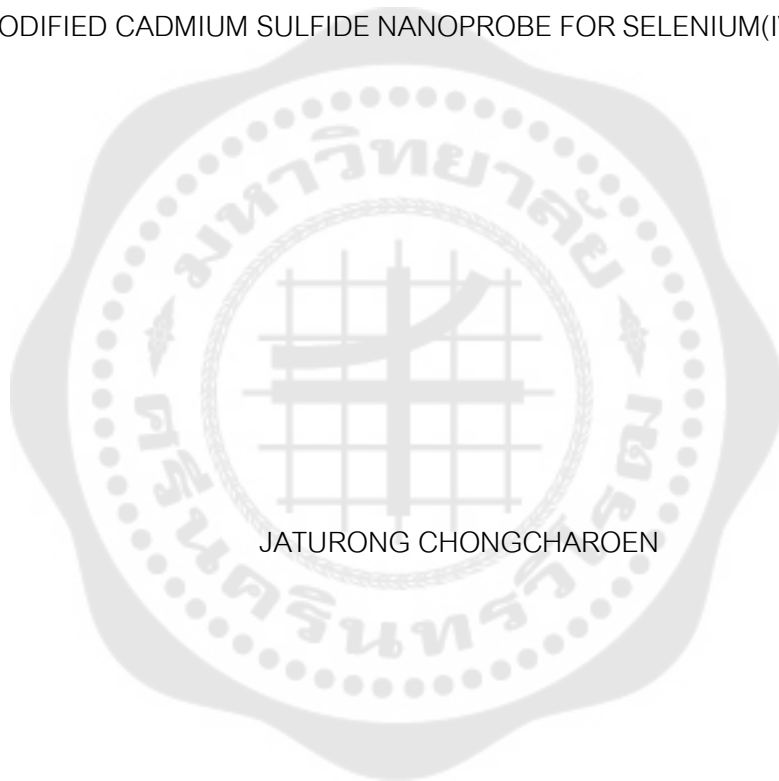




แคดเมียมซัลไฟด์นาโนโพรบที่ถูกปรับแต่งเพื่อวิเคราะห์ซีลีเนียม(IV)
MODIFIED CADMIUM SULFIDE NANOPROBE FOR SELENIUM(IV) ANALYSIS



JATURONG CHONGCHAROEN

แคดเมียมซัลไฟด์นาโนโพรปที่ถูกปรับแต่งเพื่อวิเคราะห์ซีลีเนียม(IV)



ปริญญาานิพนธ์นี้เป็นส่วนหนึ่งของการศึกษาตามหลักสูตร

ปรัชญาดุษฎีบัณฑิต สาขาวิชาเคมีประยุกต์

คณะวิทยาศาสตร์ มหาวิทยาลัยศรีนครินทรวิโรฒ

ปีการศึกษา 2562

ลิขสิทธิ์ของมหาวิทยาลัยศรีนครินทรวิโรฒ

MODIFIED CADMIUM SULFIDE NANOPROBE FOR SELENIUM(IV) ANALYSIS



JATURONG CHONGCHAROEN

A Dissertation Submitted in partial Fulfillment of Requirements
for DOCTOR OF PHILOSOPHY (Applied Chemistry)
Faculty of Science Srinakharinwirot University

2019

Copyright of Srinakharinwirot University

THE DISSERTATION TITLED

MODIFIED CADMIUM SULFIDE NANOPROBE FOR SELENIUM(IV) ANALYSIS

BY

JATURONG CHONGCHAROEN

HAS BEEN APPROVED BY THE GRADUATE SCHOOL IN PARTIAL FULFILLMENT OF
THE REQUIREMENTS FOR THE DOCTOR OF PHILOSOPHY IN APPLIED CHEMISTRY
AT SRINAKHARINWIROT UNIVERSITY

..... Dean of Graduate School
(Assoc. Prof. Dr. Chatchai Ekpanyaskul, MD.)

ORAL DEFENSE COMMITTEE

..... Major-advisor Chair
(Asst. Prof. Dr. Mayuso Kuno) (Dr. Nichanan Thepsuparungsikul)

..... Co-advisor Committee
(Assoc. Prof. Dr. PORNPIMOL MUANGTHAI) (Asst. Prof. Dr. Panarat Arunrattiyakorn)

Title	MODIFIED CADMIUM SULFIDE NANOPROBE FOR SELENIUM(IV) ANALYSIS
Author	JATURONG CHONGCHAROEN
Degree	DOCTOR OF PHILOSOPHY
Academic Year	2019
Thesis Advisor	Assistant Professor Dr. Mayuso Kuno

This research aims to develop a selective CdS-Cys-DAB fluorescent nanoprobe for the measurement of selenium(IV) in vegetable samples. The nanoprobe consisted of cysteine-capped cadmium sulfide and a modified surface with specific selenium(IV) reagent, 3,3'-diaminobenzidine (DAB). The intensity of the fluorescence emitted from the selenium-bonded nanoprobe was determined at 390 nm with an excitation wavelength at 280 nm. The TD-DFT calculations of this nanoprobe were employed using a B3LYP/6-31G(d, p) method with a Gaussian 03 package. The results revealed two strong transitions at 316.45 nm and 362.89 nm of HOMO-1 to LUMO+1 and HOMO to LUMO, respectively. The energies of the bandgap of the Cys-DAB-Se complex was found at 0.5 eV. The validation of the nanoprobe was investigated. The intensity of the fluorescence of nanoprobe showed linearity that was proportional to a quantity of selenium(IV) in the range of 1.00 - 5.00 ppm, with a correlation coefficient (R-Squared) of 0.9647. The detection limit (LOD) and quantification limit (LOQ) of this nanoprobe were 0.12 and 0.38 ppm, respectively. The results of the interfering study of some metal ions on the nanoprobe response observed a high selectivity of this nanoprobe towards selenium(IV) ions. The nanoprobe was subsequently applied to measure the selenium(IV) contents in vegetable samples. It was found that the average concentration of selenium(IV) as 0.93 μg . Based on the results, this nanoprobe should be applied for further analysis of selenium(IV) contents in other samples.

Keyword : Cadmium sulfide, Nanoprobe, Selenium

ACKNOWLEDGEMENTS

This PhD study was sponsored by the Strategic Wisdom and Research Institute for financial support for a chemical supply and Graduate School of Srinakharinwirot University. I would like to thank the Department of Chemistry, Faculty of Science, Srinakharinwirot University for instrumentation support. I am thankful to my advisor Asst. Prof. Dr. Mayuso Kuno for his advice and patience. I am grateful to my co-advisor Associate Professor Dr. Pornpimol Muangthai for her advice, patience, support, encouragement, and vision throughout this thesis study. I am thankful to Dr. Nichanan Thepsuparungsikul and Asst. Prof. Dr. Panarat Arunrattiyakorn for the signature of chairperson and committee of the oral defense of my thesis. I am thankful to everyone at the Department of Chemistry, Faculty of Science, Srinakharinwirot University for guidance during our PhD years. Finally, I will always be grateful to my mother and my sister, for her spirit, energy, and prayers, which kept me going.

JATURONG CHONGCHAROEN

TABLE OF CONTENTS

	Page
ABSTRACT	D
ACKNOWLEDGEMENTS.....	E
TABLE OF CONTENTS.....	F
LIST OF TABLES.....	I
LIST OF FIGURES.....	J
CHAPTER I INTRODUCTION	1
Background.....	1
Objectives of the research.....	2
Significance of the research	3
Scope of the research.....	3
CHAPTER II THEORY AND LITERATURE REVIEWS	4
1. Selenium.....	4
1.1 Selenium in the Environment.....	5
2.1 Toxicity of Selenium.....	9
2. Nanoparticles	11
3. Spectroscopic methods.....	14
3.1 UV-Vis spectroscopy.....	14
3.2 Fluorescence spectroscopy.....	17
4. Computational Chemistry.....	19
4.1 Type of computational chemistry method.....	19
4.2 Time-dependent density functional theory (TD-DFT).....	21

Related research.....	22
CHAPTER 3 EXPERIMENTAL.....	27
Chemical reagents and Materials.....	27
Instrumentation.....	27
Methods.....	28
1. Fabrication of the CdS-Cys-DAB nanoprobe.....	28
1.1 Synthesis of CdS Nanoparticle capped with ligand arm.....	28
1.2 Surface Functionalization of CdS Nanoparticles with DAB Molecules ..	29
1.3 Characterizations of Fluorescent Nanoprobe.....	30
2. Study effect on fluorescent nanoprobe fabrication.....	30
2.1 pH effect.....	30
2.2 Temperature effect.....	31
2.3 Fabrication time.....	31
2.4 Ion selectivity test.....	31
2.5 Ion interference test	31
3. Computational study	32
4. Analytical Performances of Development Methods.....	32
4.1 Linearity.....	32
4.2 Precision.....	32
4.3 Limit of Detection	33
4.4 Recovery Studies	33
4.5 Statistical Analysis.....	33
5. Application on Determination of selenium in samples.....	34

CHAPTER 4 Results and Discussion	35
1. Fabrication of the CdS-Cys-DAB nanoprobe	35
1.1 Synthesis of CdS Nanoparticle capped with ligand arm	36
1.2 Surface Functionalization of CdS Nanoparticles with DAB Molecules	39
1.3 Characterizations of CdS-Cys-DAB Nanoprobe	41
2. Study effect on fluorescent nanoprobe fabrication	44
2.1 pH effect condition	44
2.2 Temperature effect condition	45
2.3 Fabrication time	47
2.4 Ion selectivity effect	47
2.5 Ion interference effect	48
3. Computations study	49
4. Analytical performance of CdS-Cys-DAB nanoprobe	51
5. Application on Determination of selenium(IV) in samples	52
CHAPTER 5 Conclusions and Recommendation	54
REFERENCES	56
APPENDIX	62
GLOSSARY	70
VITA	72

LIST OF TABLES

	Page
Table 1 Se-compounds in a plant.	9
Table 2 Relationship between wavelength field region and colors of light.	16
Table 3 Fluorescent intensity of ligands arm capped.	39
Table 4 Table of the solution pH effect on the fluorescence intensity of the CdS-Cys-DAB nanoprobe-Se(IV) complex.....	44
Table 5 Table of the solution temperature effect on the fluorescence intensity of the CdS-Cys-DAB nanoprobe-Se(IV) complex.....	46
Table 6 the error percentage of the ion interference effect study.	49
Table 7 Excitation wavelength forms calculation and experimental methods.	51
Table 8 The analytical performance of CdS-Cys-DAB nanoprobes.....	52
Table 9 Results of selenium determination (n = 3) in raw vegetables	53

LIST OF FIGURES

	Page
Figure 1 Selenium by-product from silver and gold refining process.	5
Figure 2 Description of selenium species pathways and soil, water, atmosphere, and interface transformations.	6
Figure 3 Selenium distribution in soil according to pH and redox potential.	7
Figure 4 Major selenium routes at the interface between the soil-plant-atmosphere.	8
Figure 5 Diagram of different forms of selenium contained in a plant.	9
Figure 6 Production methods for nanoparticles: top-down and bottom-up.	11
Figure 7 Photoexcitation mechanism and the recombination of radiative electron-hole (fluorescence).....	13
Figure 8 Electric field and magnetic field.	15
Figure 9 Schematic diagram of the electromagnetic spectrum.	16
Figure 10 Electronic transition.....	17
Figure 11 The Jablonski Diagram of fluorescence and molecular absorption	18
Figure 12 Formula structure of 2,3-diaminonaphthalene.....	22
Figure 13 The formula structure of 3,3'-diaminobenzidine (DAB).	23
Figure 14 Ligand (2-(2-(2-aminoethylamino)ethyl)-3',6'-bis(ethylamino)-2',7'-dimethylspiro[isindolin-1,9'-xanthen]-3-one) synthesis route.....	24
Figure 15 Turn-on fluorescent nanoprobe producing schematic diagram for selenium determination(IV).	25
Figure 16 The MS1 (top) and MS1-Hg ²⁺ (bottom) DFT-optimized structures; red atom, O; atom blue, N; atom gray, Hg.	25

Figure 17 Schematic diagrams of TD-DFT / B3LYP / LANL2DZ calculated transitions of complex electronic absorption.....	26
Figure 18 Schematic diagram of two distinct solutions to monodispersed spherical metal colloids, (A) bottom-up and (B) Top-down methods.	36
Figure 19 Growth mechanism of CdS nanoparticles.	37
Figure 20 Illustrates of CdS nanoparticle capped with 3 types of ligand arms, (A) capped with DMSA, (B) capped with MPA, (C) capped with L-cysteine.....	38
Figure 21 Structure of 3,3-diaminobenzidine (DAB) molecule	39
Figure 22 Structure of (A) 1-ethyl-3-(3-dimethyl aminopropyl) carbodiimide hydrochloride (EDC) and (B) N-hydroxysuccinimide (NHS) molecule	40
Figure 23 Scheme of crosslinking reaction of Sulfo-NHS and EDC (carbodiimide)	40
Figure 24 Schematic diagram shows the fabrication of the CdS-Cys-DAB nanoprobcs used to determine selenium(IV). (A) CdS-Cys nanoparticle. (B) DAB modified on CdS-Cys nanoparticle for selenium measurement.	41
Figure 25 CdS-Cys nanoparticles SEM and TEM images (A and B). TEM images of nanoprobcs (C) operated by CdS-Cys-DAB.	42
Figure 26 (A) CdS-L-cysteine nanoparticles fluorescent emission spectrum, (B) CdS-Cys nanoparticles with the presence of Selenium(IV), (C) CdS-Cys-DAB nanoprobcs and (D) CdS-Cys-DAB nanoprobcs in the present of Se(IV) present. The excitation wavelength was set at 280 nm.	42
Figure 27 The illustrate of the EDS spectrum as 1. (A) bare nanoprobcs and 2. (B) captured with Selenium(IV)	43
Figure 28 The solution pH effect on the fluorescence spectrum of the CdS-Cys-DAB nanoprobe-Se(IV) complex.	45
Figure 29 The solution pH effect on the temperature spectrum of the CdS-Cys-DAB nanoprobe-Se(IV) complex.	46

Figure 30 The fluorescent intensity dependence for CdS-Cys-DAB synthesis time.....	47
Figure 31 Comparison of the CdS-Cys-DAB nanoprobe responses to the selenium ion for common metal ions.	48
Figure 32 Effect of foreign interference ions on functional CdS-Cys-DAB nanoprobe fluorescence intensity.....	48
Figure 33 The optimized structure of Cys-DAB-Se complex.....	50
Figure 34 The LUMO and HOMO frontier molecular orbital amplitude plots of this probe by Gaussian process B3LYP/6-31G(d, p).	50
Figure 35 The linear regression range of CdS-Cys-DAB nanoprobe.....	51
Figure 36 Spectrum of QD-DAB-Se form fluorescence spectrophotometer Model: Jasco, code FP-6200 PC (USA).....	63
Figure 37 Spectrum of DAB-Se form fluorescence spectrophotometer Model: Jasco, code FP-6200 PC (USA).....	63
Figure 38 Spectrum of CdS-DAB form fluorescence spectrophotometer Model: Jasco, code FP-6200 PC (USA).....	64
Figure 39 Spectrum of CdS form fluorescence spectrophotometer Model: Jasco, code FP-6200 PC (USA).....	64
Figure 40 TEM image of CdS core particle.....	65
Figure 41 TEM image of CdS core particle after immobilized.....	65
Figure 42 SEM image of CdS core particle.	66
Figure 43 SEM image of CdS core particle after immobilized with DAB.....	67
Figure 44 Setting of Synthesis of CdS-Cys-DAB nanoprobe.....	67
Figure 45 Precipitation effect at high pH and high temperature	67
Figure 46 Fluorescent property in UV-lamp after synthesis finally.	68
Figure 47 Precipitated by addition of ethanol and solvent (water)	68

Figure 48 Shallot, garlic and onion sample for selenium(IV) analysis..... 69



CHAPTER I

INTRODUCTION

Background

Selenium is a necessary nutrient; it plays an essential in human activity (1). Selenium also presents in human bodies as selenoproteins used in cellular metabolism (2). Selenium deficiency has been shown to affect human health. For example, a decrease in the role of the immune system and thyroid function, high risk for cancers as prostate cancer, breast cancer, Kashin-Beck disease and cancer (3). Albeit selenium is an important substance, It is harmful if the concentration reaches the level of safety. Generally, the human body requires selenium approximately 0.10 to 0.30 $\mu\text{g}/\text{kg}$. When receipt a higher selenium concentration (2.00 to 10.00 $\mu\text{g}/\text{kg}$). It will result in produces chronic toxic symptoms such as cirrhosis, liver carcinoma, paralysis and loss of teeth. Therefore, the United States of America (USA) was prescribed a daily allowance of 55.00 μg / day selenium content for humans.

Because of selenium's physiological importance, It is very important to measure the concentration of selenium. There have several methods for assessing trace levels of selenium, such as Atomic spectrometry, Fluorometry, Stripping Voltammetry, and Mass spectrometry (4). Some of these methods can detect selenium that is highly sensitive. Nonetheless, the method of detection is very important for some environmental and food samples.

Fluorescent nanomaterials are innovation materials for evaluating trace amounts of targets sensitively and selectively (5). Several types of fluorescent nanomaterials, such as plasmonic nanoparticles, quantum dots and magnetic nanoparticles (6). Fluorescent nanoparticles have been commonly used as replacements for molecular fluorophors in biomedical applications. Compared to traditional fluorescent molecules, these fluorescent nanomaterials exhibit excellent photostability and high sensitivity to signal target traces. However, the fluorescence of these nanomaterials is intrinsic and their fluorescence frequency does not alter as the targets are connected to the nanomaterials. Such fluorescent nanomaterials can therefore only be used as

a fluorescent labeling reagent, but not as a target binding in-situ probe. For addition, because of the fluorescence, for the presence of analytes, it is permanent and not "turned on", the removal of unbound fluorescent nanomaterials from the analyst matrix involves a separation step. This step should reduce signals from the background.

The accumulation of selenium in *Allium* species has been well reported (7). A suite of unique organosulfur compounds found in the different vegetable of *Allium* species such as onion (*Allium cepa*) and garlic (*Allium sativum*), It has medicinal properties, including chemopreventative properties (8), cardiopreventative (9) And other impacts on nutrition, demonstrates that selenium-enriched vegetables could be a better source of organoselenium analogs than normally used selenite or selenomethionine.

In this study, we focus on the preparation of fluorescent nanomaterials to be a nanoprobe, with a target-induced signaling capability for in situ selenium detection and no separation step required. The purpose of this nanoprobe is to immobilize of 3,3'-diaminobenzidine molecules on the surface-modified cadmium sulfide nanoparticle. The 3,3'-diaminobenzidine molecules show a few fluorescence intensity. After surface modification was developed to capture Se(IV), the higher intensity of the fluorescence is represented form complex of 3', 4'diaminophenylpiazselenol (10). The emission intensity depends on the amount of selenium on the surface of the nanoprobe; thus, the monitoring of selenium can be achieved using this nanoprobe. In this method, no separation process is required to reduce background fluorescence signals. After surface modification, we will make the probe to measure the amount of selenium in the *Allium* species sample. It also depends on how fluorescent nanoprobe are designed to track a wide variety of other samples in the future.

Objectives of the research

1. To synthesize cadmium sulfide nanoparticle and the modified surface of cadmium sulfide nanoparticle for specific selenium(IV) detection.
2. To study the binding site optimize conditions for fluorescent nanoprobe for determination selenium(IV) and study the effects of selenium analysis.
3. To apply nanoprobe for analysis selenium(IV) in a sample.

Significance of the research

1. Obtain synthesis conditions and modified surface procedure of cadmium sulfide nanoparticle for the determination of selenium(IV).
2. Obtain the optimum conditions for synthesis nanoprobe.
3. Obtain the selenium(IV) concentrations with this developing nanoprobe in samples.

Scope of the research

1. Synthesis of new modified surface cadmium sulfide nanoprobe.
2. To study an effect and conditions for optimizing synthesis and surface modification of cadmium sulfide nanoparticle. Such as pH effect, synthesis time and synthesis temperature and other metal interferences.
3. Application this developing the method for selenium(IV) analysis in samples.

CHAPTER II

THEORY AND LITERATURE REVIEWS

In this study, the nanoprobe sensor for determination selenium in samples was prepared using many chemical reactions and proven by computational chemistry. The general information and related works were explained as the following themes.

1. Selenium
 - Selenium in the environment
 - Toxicity of Selenium
2. Nanoparticles
3. Spectroscopic methods
 - UV-Vis spectroscopy
 - Fluorescence spectroscopy
4. Related research

1. Selenium

Selenium is non-metal with 34 atomic numbers and 78.96 Daltons atomic weight. The crystalline selenium has a melting point of 217 °C and a boiling point of 685°C. Selenium will change to strong acid as selenous acid (H_2SeO_3) when it reacts with water. The acids salts of selenium such as selenites (oxidation states: + 4) and selenates (oxidation states: +6) soluble in water. Selenium is an active component that interacts easily with hydrogen, fluorine, chlorine, bromine and other metals.

However, selenium is a very rare element and generally found as a sulfide mineral by-product and other metal-refining industries (Figure 1). The major production of selenium comes from Japan, Canada, Belgium, United States and Germany (U.S. Geological survey 2012). Selenium has many forms of commercial products, such as selenium oxychloride, selenium dioxide, sodium selenate, and sodium selenite.

Selenium has been used in many industries, including mining, fossil fuel combustion, metal processing, metallurgy, batteries, food, electronics, and cosmetics so that selenium can be converted into the environment.

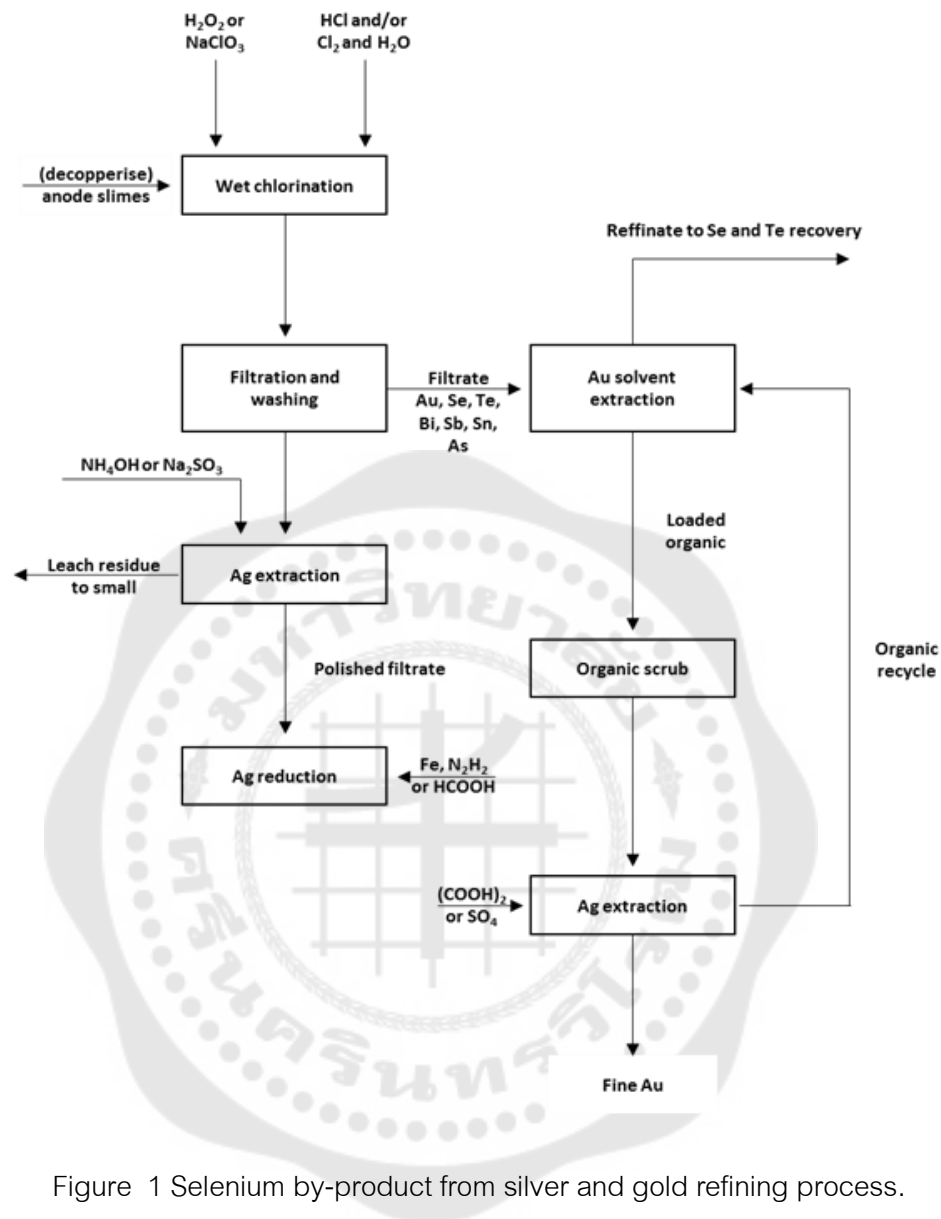


Figure 1 Selenium by-product from silver and gold refining process.

Source: Adapted from Soldenhoff. (11)

1.1 Selenium in the Environment

Selenium is one of the rarest elements on this earth's surface. Figure 2 provides the most significant schematic description. Selenium in soil, water, and air showing the major biogeochemical pathways through interfaces. Sulfide ores, pyrite, and high-sulfur coals are the main selenium reserves on earth. Volcanic eruptions are burning and releasing selenium into the air, which exists in selenium(IV) oxide form. Selenium is also

as selenate (SeO_4^{2-}), selenite (SeO_3^{2-}), selenide (Se^{2-}) and elementary selenium (Se^0). Selenate and selenite in cultivated soils (17) form aeration, hydrological regime and other soil reaction (18). effect on the type of selenium compounds. An individual form of selenium in a soil undergoes regulated transformations with processes of oxidation-reduction. Figure 3 shows the dependence of the form of selenium on pH and redox potential.

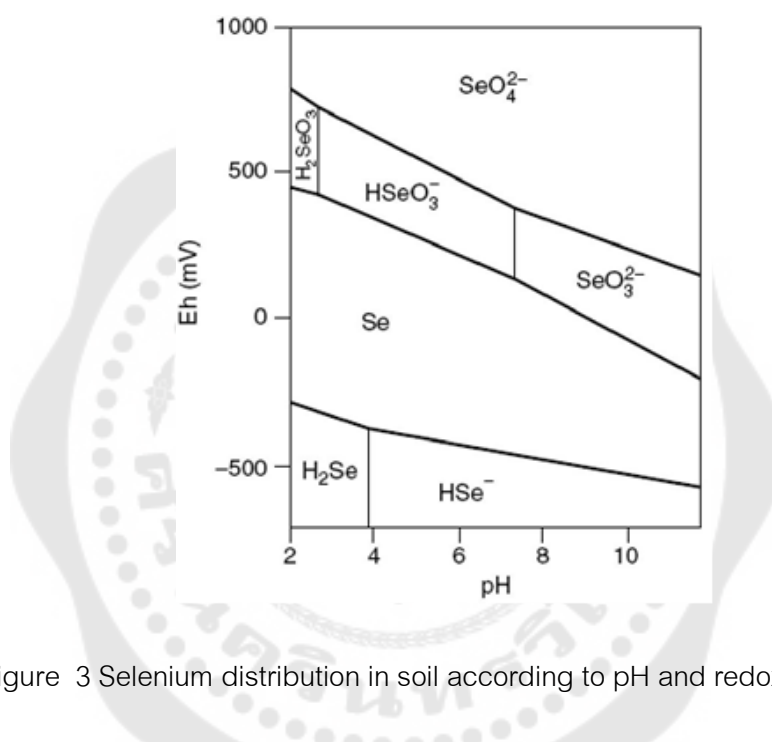


Figure 3 Selenium distribution in soil according to pH and redox potential.

Source: Jezek and coworkers. (16)

In plants, selenium is highly water-soluble and easily leachable to plants. Plants absorb selenium as selenite, selenate and selenium-amino acid such as selenium-methionine (Se-met). Certain forms of selenium such as elementary selenium (Se^0), selenides (Se^{2-}) and selenium (Se^-) are normally in an environment's reduced state, but can not be contained in plants. The selenium ions transported almost quickly to the surface of the roots through the mechanism of mass flow, resulting from the plant receives water. Diffusion is selenium's main transportation method in the soil. In general, by passive or active mechanism, almost ions reach the roots of the plant. The transfer of selenite and organic selenium against an electrochemical gradient to the root.

The transmitter of sulfate ions (SO_4^{2-}) is also involved in selenite uptake. The selenite absorption process is regulated positively by O-acetylserine and negatively regulated by sulfate and glutathione (Figure 4).

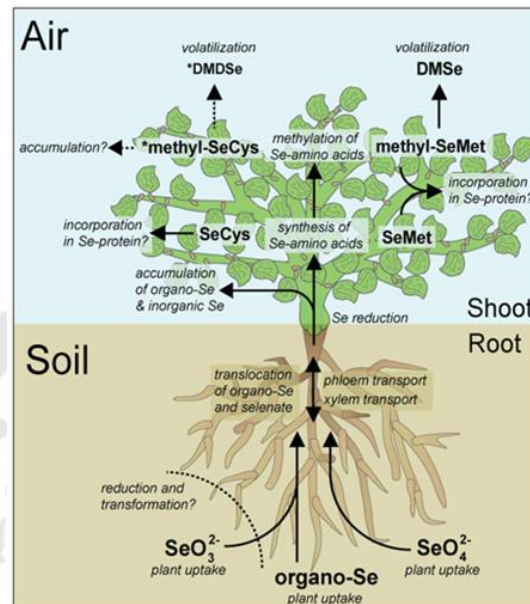


Figure 4 Major selenium routes at the interface between the soil-plant-atmosphere.

Source: Winkel and coworkers. (13)

Sulfur metabolism transformation and assimilation of selenium in plants (Figure 5). Most enzymes are involved in sulfate and selenite reduction. The enzyme-catalyzed reactions with the sulfate adenylyltransferase enzyme (ATP-sulfurylase) result in intermediate phosphosulfate reduction. Glutathione (GSH) has reduced selenite to selenotrisulphide (GSSeSG). Selenotrisulphide will then be reduced to selenoglutathione (GSSeH) and Se^{2-} . In the reduction of GSSeSG and GSSeH, Coenzyme NADPH interacts with O-acetylserine (O-AS) and produces selenium-cysteine in reducing GSSeSG and GSSeH. Selenium-cysteine is a precursor of Se-met synthesis that can be transformed into the structure of other selenium-compounds by subsequent metabolic processes. In conclusion, selenium-compounds are mentioned in plants shown in Table 1.

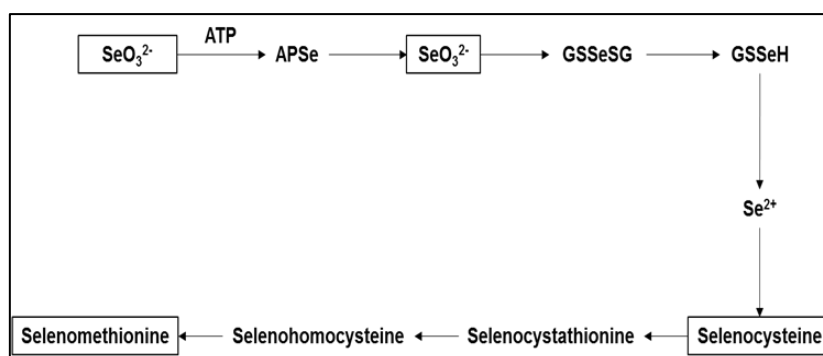


Figure 5 Diagram of different forms of selenium contained in a plant.

Source: Adapted from Eich-Greatorex and coworkers. (19)

Table 1 Se-compounds in a plant.

Se-compounds		
Selenate	Selenocysteineselenic acid	Se-propylselenocysteine
Selenocystine	Dimethyl diselenide	Se-methylselenocysteine
Selenite	Se-proponylselenocysteine	Selenopeptide
Se-cysteine	Selenocystathionine	Selenohomocysteine
Se-methionine	Se-methylselenomethionine	Dimethylselenide

Source: Jezek and coworkers. (16)

2.1 Toxicity of Selenium

Selenium has some nutritional functions of concern. It is essential for the health of plants and animals in very small amounts (less than 55 µg) (20). Selenium is the necessary part of the amino acids such as cysteine and methionine to form selenocysteine and selenomethionine, respectively. In animals that have low levels of selenium in their diets, weak muscles can develop. Selenium is an antioxidant enzyme

including glutathione peroxidases and thioredoxin reductase in humans (21). This assists in the thyroid gland's daily functions. Selenium deficiency can lead to potentially fatal Keshan disease. Keshan disease contains signs such as myocardial necrosis which leads to heart disease. If a diet is low in selenium and iodine, Keshan-Beck disease may develop, leading to immune deficiency, which makes the body less resistant to dietary, biochemical and infectious diseases (22). Selenium is required for thyroid hormone thyroxine (T₄) to be transformed into triiodothyronine. A selenium deficiency causes hypothyroidism, leading to extreme fatigue, mental slowing, goiter, cretinism, and miscarriage. Some research has shown a higher incidence of HIV / AIDS in locations around the world with low levels of selenium in the soil. Selenium deficiency is strongly correlated with AIDS progression and death risk (23).

Selenosis illnesses may occur in the case of intake selenium exceeding 400 µg per day. The illnesses include neurological damage, gastrointestinal disorders, hair loss, gastrointestinal disorders clogging, tiredness, clogging and irritability. (24). Hepatic cirrhosis, pulmonary edema, and death can occur with excessive selenium concentrations. Several case reports have been published on acute selenium toxicity in humans. Some traditional cases such as the five men ingested turkey feed supplement with large amounts of selenite are described. All men vomited and suffered from abdominal pain, tremors shortly, diarrhea, chills, and abdominal pain after ingestion. (25). A 35-year-old woman eats around 10 g of an unidentified type of selenium-containing breakfast cereal (35 mg per gram). A year later, after her consumption, she vomited, nausea, cramps and felt numbness in her arms within 30 minutes. She recovered within days, but later experienced irregular menstrual bleeding and marked hair loss. Her hair analysis (by neutron activation) was performed 13 months later. That was shown the amount of selenium was about 0.50µg per gram (25). Another case as a criminal poisoning has been reported. A 46-year-old man was admitted several times to the hospital. He complained about the sudden onset of abundant watery diarrhea and vomiting. He lost his scalp hair and noticed a strong smell of garlic.

His fingers also had a purple-red discoloration. The criminal investigation later revealed that his wife had a medical tool including selenous acid (26).

2. Nanoparticles

Nanomaterials are now increased in recent years. Because of their unique physical and chemical properties, new avenues of technological, environmental and biological applications are expected to open up. Such nanomaterials are used in catalysts, semiconductors, detectors, drug carriers, and products for personal care. Nanoscience and nanotechnology are thought to be a revolution that is expected to have huge impacts on human life in the near future. In the coming years, commercial products containing synthetic nanomaterials are expected to increase significantly (27). Nanotechnology is developing, functionalizing, characterizing and using nanometer-sized materials. Nonetheless, the term "nanoparticles" refers to materials below 1000 nm, but in the nanotechnology field, nanoparticles used in the range from 1 to 100 nm. (28). The nanomaterials are subject to the universal laws of the universe, although they have properties that differ from those of their bulk counterparts. The main reasons behind this are the marginal consequences, which can be overlooked on a large scale. The effect of nano-scale on quantum properties and the high surface area to volume field (27). Nanoparticles can be prepared using methods of varieties that are typically classified into two major synthetic paths, the top-down and bottom-up approaches (Figure 6).

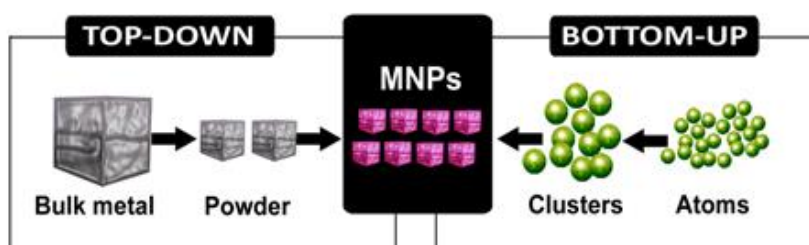


Figure 6 Production methods for nanoparticles: top-down and bottom-up.

Source: Laboratory for micro and nanotechnology. (29)

In the top-down pathway, nanoparticles are made from their bulk materials using various methods and techniques, such as lithography and photoablation. Contrary to bottom-up synthesis, the nanoparticles are derived from their basic atoms or molecules to produce the desired shape and size of the nanoparticles (30). Nanoparticles are made from a variety of materials, including biomolecules, organic and inorganic. The nanoparticles could be divided into three major groups.

Plasmonic Nanoparticles, Plasmonic nanoparticles are an inorganic class that is very important due to their various applications from sensing and catalysis to biological applications (31). Attributed to their special electronic and optical features, in particular, localized surface plasmon resonance (LSPR). In physical, the oscillation of a quasi-free electrons gas is referred to as plasmon. The resonance of the surface plasmon is the consistent collective oscillation of free electrons in the conduction band because of the coherent excitation of free electrons caused by the electromagnetic field interaction. The electromagnetic light interacts with the plasmonic nanoparticles in matches with the frequency of the oscillating electrons, The incident photon frequency resonates with the electrons collectively oscillating in the conduction band. This creates a collective oscillation of electrons in resonance with the frequency of incident light, so this is known as Localized Surface Resonance (LSPR) on the nanoparticle surface (32). LSPR creates a strong band of absorption and scattering.

Quantum Dots, quantum dots (QDs) are highly fluorescent semiconductor nanocrystals, also referred to as artificial atoms, are the consequence of the so-called quantum size effect. They have a unique optical and electronic property in their composition, small size, and size-tunable. The quantum dots capable of absorbing light at a shorter wavelength than the power of the bandgap, and emit fluorescence light. But in a color light that is about the same as the energy of bandgap. Certain characteristics of emission spectra are narrow and symmetric. Furthermore, photobleaching is largely reduced compared to common organic fluorophores (33). The special properties of the quantity dots are due to changes in state density and the quantum confinement associated with the size reduction of the diameter nanoscale below the Bohr radius.

Moving from bulk materials to smaller and smaller sizes that exceed certain dimensions. If the size is small enough, The charging carriers (electrons and holes) within the particle begin to recognize particle volume limitations (walls) and the spatial distribution of charging carriers within the particle are confined to a limited volume in a phenomenon known as quantum confinement. As with the bulk semiconductors when the energy of the incident photons is greater or equal to the energy of the bandgap (Figure 7). The electrons are photo-excited from the valence band to the conductive band creating an electron state and hold (the so-called exciton). The coulombic interactions also demonstrated between the negatively charged electron and the positively charged hole. In processes known as electron-hole recombination, the excited electrons can relax back to the valence band, which could generate a radiation wavelength. In either recombination of radiation or non-radiation, A photon of certain energy is emitted that corresponds to the material bandage. The energy of the emitted photon (wavelength) depends on the size of the quantum dots material. This process explains why quantum dots can absorb all wavelengths that are greater than their bandgap and turn them into a single color. Recently, a rapidly growing interest has been paying to exploit the unique properties of quantum dots nanocrystals in various applications such as light-emitting diodes and solar cell, sensing, branding, imaging, and therapeutic optoelectronics and biological applications (33)

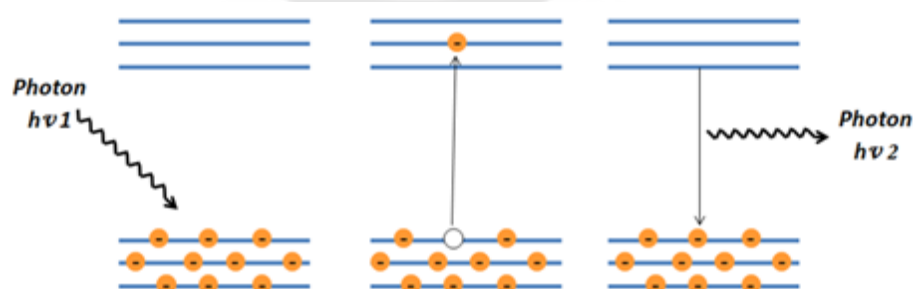


Figure 7 Photoexcitation mechanism and the recombination of radiative electron-hole (fluorescence).

Source: Abdelmonem and coworkers. (34)

Magnetic nanomaterials, Magnetic nanoparticles are a very interesting group of nanomaterials due to their special and flexible magnetic properties which differ significantly from their bulk materials. The magnetism derives from the electron spin (spin magnetic moment) and the electrons ' orbital motion (orbital magnetic moment) around the nucleus. The magnetic moment for an atom as a whole is the sum of all orbital and spin magnetic moments in the atom. All materials are magnetic and reveal some magnetic response which varies between different materials in many order of magnitude. Based on their responses to magnetic properties, Products may be categorized as paramagnetic, diamagnetic, antiferromagnetic or ferromagnetic. The magnetic fluids are homogeneous colloiddally stable suspensions produced of magnetic nanoparticles suspended in solvent (organic or aqueous solvent). Each of the magnetic nanoparticles has a surfactant that provides the colloidal stability that prevents the nanoparticles from aggregating (35).

The magnetic nanoparticles have been extensively studied in several technical and biological applications because of their properties, such as small size and superparamagnetic behavior. (36)

3. Spectroscopic methods

Spectroscopic techniques are applied in all the scientific and technological fields. Spectroscopy is the study of matter absorption and light emission and other radiation, related to the wavelength of the radiation dependence of these processes. UV-Vis spectroscopy and fluorescence spectroscopy can be used to analyze the physical properties of substances.

3.1 UV-Vis spectroscopy

Electromagnetic radiation includes an electrical field and a perpendicular magnetic field. (Figure 8).

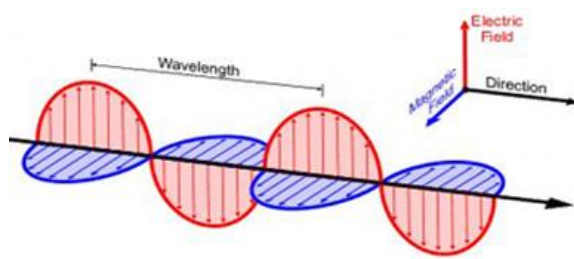


Figure 8 Electric field and magnetic field.

Source: Physical Methods for Chemists. (37)

In the electromagnetic spectrum, the absorption and release of energy happen within discrete photons. The relation between the photon's energy, the frequency and wavelength are shown in equations 1 and 2.

$$E = h\nu \quad \text{----- [1]}$$

$$\nu = \frac{c}{\lambda} \quad \text{----- [2]}$$

Where,

- E is energy.
- h is Planck's constant (6.626×10^{-34} J s).
- ν is frequency (s^{-1}).
- c is the light speed in a vacuum (2.9979×10^8 m s^{-1}).
- λ is wavelength (nm).

The various regions in the electromagnetic spectrum are displayed with the nature of the change brought about by the radiation (Figure 9). The ultraviolet region is in the range of 200-380 nm, while visible light is generally considered to extend from 380-780 nm (Table 2).

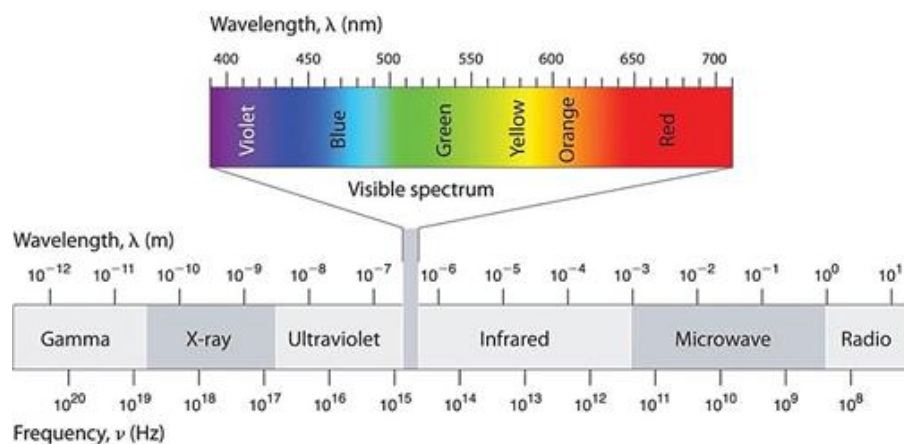


Figure 9 Schematic diagram of the electromagnetic spectrum.

Source: Instant Notes: Physical Chemistry. (38)

Table 2 Relationship between wavelength field region and colors of light.

Wavelength region (nm)	Transmitted color
< 380	Ultraviolet
380-435	Violet
435-500	Blue
500-560	Green
560-580	Yellowish green
580-595	Yellow
595-650	Orange
650-780	Red
> 780	Near-infrared

Source: Instrumental Methods of Analysis. (39)

Absorbance is observed when light energy is used to promote electrons of the molecule from the ground state to the excited state, when the electrons in the excited state return to the field, fluorescence emission is observed. This phenomenon is called electronic transition (Figure 10).

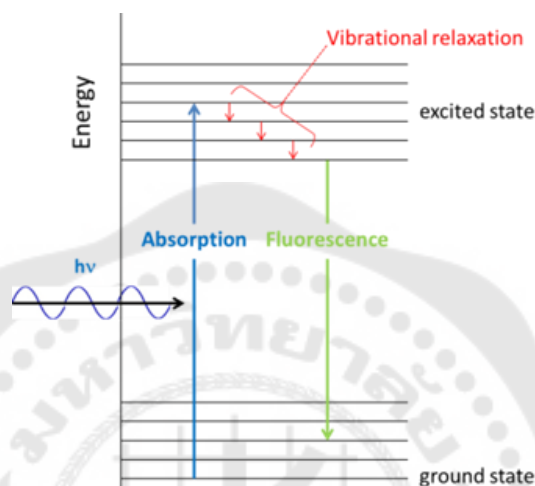


Figure 10 Electronic transition.

Source: The Elements of Physical Chemistry. (40)

3.2 Fluorescence spectroscopy

Fluorescence spectrometry is a quick, cheap and easy method for determining an analyte's concentration in a solution based on its fluorescent properties. The quantitative analysis to determine the concentration of the analytes can be used for relatively simple analytes, where the type of compound to be analyzed is known. Fluorescence is mainly used in solution measurement of compounds.

Figure 11 shows the diagram of Jablonski (41), Schematic of the electronic molecule transition during the fluorescence phenomenon. The left axis displays rising energy where a standard fluorescent molecule has a spectrum of absorption. This spectrum displays the wavelengths or energy, Wherever the molecule absorbs light. The emission of fluorescence is caused by the transition of photons from a single electronic excited state (S_1) to a single electronic ground state (S_0). Then the electrons

go through internal conversion, affecting the environment with vibrational relaxation and heat loss. It then emits a photon in the form of fluorescence from the lowest singlet excited state. The lifetime of fluorescence is about 10⁻⁹ minutes.

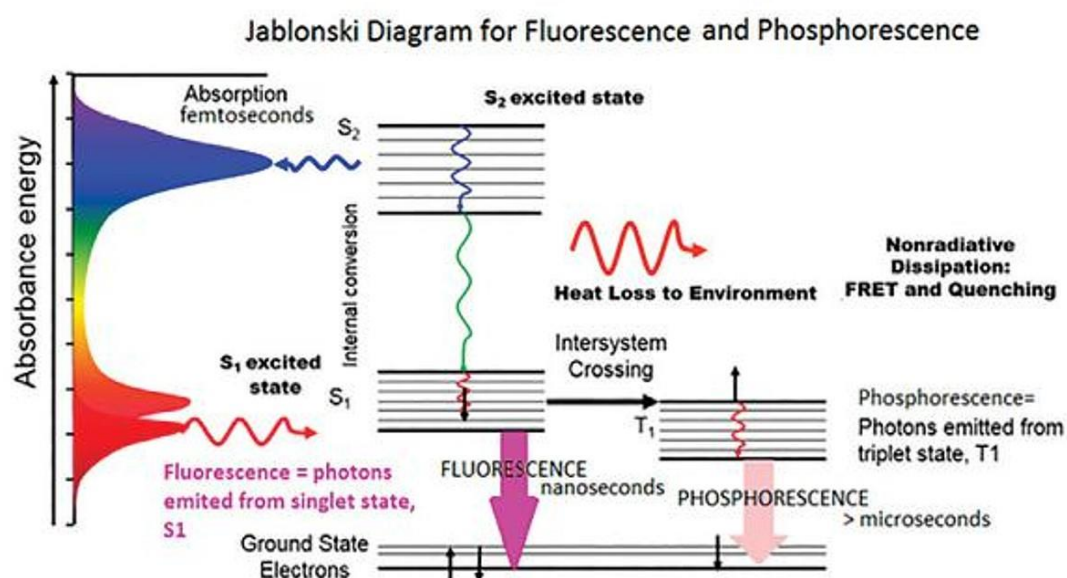


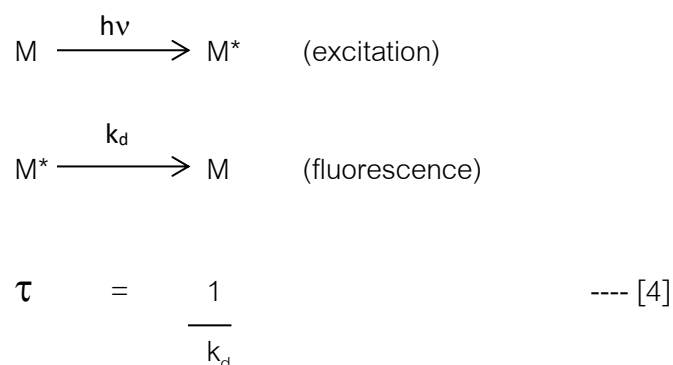
Figure 11 The Jablonski Diagram of fluorescence and molecular absorption

Source: The Jablonski diagram. (41)

The fluorescence quantum yield (Φ) is an indicator of occurring effective fluorescence, as shown in equation 3.

$$\Phi = \frac{\text{Fluorescence}}{\text{Absorbance}} \quad \text{---- [3]}$$

In simple terms, the lifetime of a molecule's fluorescence is the average amount of time it spends in the excited state. It depends on the form and local environment of the molecule. The fluorescence lifetime (τ) is inversely proportional to the excited state decay rate constant (k_d), as shown in equation 4.



In fluorescence spectroscopy, a beam with a wavelength ranging from 180 to 800 nm passes through a solution in a cuvette. In fluorescence spectrometry, it is possible to measure both an excitation spectrum (the sample-absorbed light) and/or an emission spectrum (the sample-emitted light). The analyte concentration is directly proportional to the emission intensity.

The intensity and shape of the spectra are influenced by several parameters. When recording a spectrum of emissions, the intensity depends on the wavelength of excitation, the analyte solvent concentration, the cuvette size of the path, the sample self-absorption effect.

4. Computational Chemistry

The theory of electronic structure is the application of quantum mechanics in the calculation of molecular structure and properties. In terms of exactly solving the Schrödinger wave equation (SWE), applying the principles of quantum mechanics to molecular properties is challenging. The various theoretical models were developed to solve the SWE approximately. Comprehending the strengths and weaknesses of these approaches is the secret to target molecules applications. Factors in the selection of the method include the size of the molecules being studied and available computational resources.

4.1 Type of computational chemistry method

Molecular Mechanics (MM), MM is calculating target species properties as a function of a nuclear position (42). Classical physics can explain the motion of the

atoms by neglecting the momentum and position of the electrons. Such approximations make MM calculations much quicker and less costly than the methods based on quantum mechanics (QM). Parameters for each type of atom are precisely defined in MM based on its hybridization and coordination number. Force field parameters are used to measure the molecule's total energy as a total of the interactions between bond stretching, bond torsion, angle bending, electrostatic and van der Waals. The MM-based conformational search was performed in this research for species with a large number of potential conformations, i.e. complexes with many rotatable bonds. The resulting conformations are then optimized at higher theoretical scales.

Semi-empirical quantum mechanics (SEQM), SEQM is the method that uses fewer parameters than MM methods. Furthermore, SEQM methods consider only valence electrons and ignore other components of electron-electron interaction that are known to be small in size. For these reasons, SEQM methods are much faster than the theory (including DFT) but slower than MM techniques. The predicted computational trade-off for SEQM versus MM techniques is more accurate. PM3 (parameterization method 3 for transition metals) is used in this research among several SEQM methods. The PM3 method uses a minimum valence base set of Slater type orbitals and subsequently, the parameters are expanded to transition metals.

Ab Initio Methods, Ab initio is an electronic structure method to solve the Schrödinger wave equation (SWE) using the laws of quantum mechanics. Although many mathematical approximations are applied, it is computationally impossible for most systems to find an exact solution for the SWE equation. The two most important approaches developed for molecular systems are Hartree-Fock (HF) and Density Functional Theory (DFT).

Density functional theory (DFT) (43), DFT is probably the most commonly used method in the theory of transition metals in electronic structures. This theory was initially developed by Hohenberg and Kohn. In their theory, the energy of a device can be obtained from its density of electrons. In other words, the electron density precisely defines the energy and all the properties of the ground state of a molecule for a given

set of nuclear coordinates. There are several uses and advantages of DFT approaches. The accuracy of DFT calculations is often comparable to higher post-HF methods, While the cost of computation is equivalent to HF calculations.

Hybrid Methods, Hybrid methods combine two or more different theory levels, each of these applied to specific regions of concern of the chemical organism. In these studies, by using QM / MM methods, large molecules with many atoms are investigated. The methodology of ONIOM (our integrated molecular orbital n-layer + molecular mechanics) was used. The central transition metal, metal-connected atoms or atoms in conjunction with these are modeled on QM techniques. The remaining atoms in the complex are treated with MM force fields, typically far from the transition metal (or reaction center).

“Basis sets” are mathematical functions representing electrons movement and location. Throughout modern computational chemistry, quantum chemical calculations are typically performed with a finite basis-set function centered within the molecule at each atomic nucleus. Due to computational considerations, these basic functions are usually Gaussian orbitals (GTO). For most of the calculations mentioned in this study, the Gaussian 09W (G09) code is used.

4.2 Time-dependent density functional theory (TD-DFT)

The DFT has been shown to be applicable with some effective exchange-correlation functional for a fictitious, non-interacting electron system that provides an efficient method for treating the ground-state properties of multiple electron systems such as solids and molecules. Unfortunately, The excited states measured using the Kohn-Sham method are not as effective for time-dependent disturbances like optical response and excitation spectrum. This ground-state DFT time-dependent analog is called the time-dependent functional density theory (TD-DFT) and was first formally proved (under certain general conditions) (44). The extension of the DFT formalism in the ground-state shows that there is a one-to-one correspondence between the time-dependent density $\rho(r, t)$ time-dependent potentials $V_{\text{ext}}(r, t)$ for the initial condition in question. In addition, TDHF's initial applications to atomic systems predated TD-DFT's

formal design (45). The functional theory of time-dependent density (TD-DFT) is a quantum mechanical concept used in physics and chemistry to investigate the properties and dynamics of multiple body systems with time-dependent potential, For example, electrical or magnetic fields.

Related research

Selenium, as described above, is an essential element and is also a toxic element. There are different analytical techniques in environmental samples for the determination of selenium species. The selenium identification in environmental samples as a result of selenium fading in speciation. The trace quantity of selenium in biological and environmental samples requires a sensitive analytical technique. The most analytical methods are also focused on preliminary steps in sample preparation such as acid digestion/separation, so this step is very critical before determining the overall selenium content. In studies published such as spectrophotometry, atomic absorption spectrometry (AAS), inductively coupled plasma (ICP-AES, ICP-MS), various analytical techniques were used to measure selenium.

In 1966, Wilkinson and coworkers (46) reported selenium(IV) concentrations level in biological material base on spectrofluorometric technique. Selenium reacts with 2,3-diaminonaphthalene (DAN) (Figure 12) in the present as a catalyst of bromide ions, to form the DAN-Se complex which can be extracted by cyclohexane in an acid environment. The DAN-Se complex gives a strong fluorescent signal at 376 nm. This approach produced a linearity of 0.02 to 0.024 μg , relative standard deviation (RSD) as 3.6%, and percentage recovery as 101%.

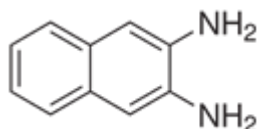


Figure 12 Formula structure of 2,3-diaminonaphthalene.

In 1989, Handyman and coworkers (47) used DAB for extraction selenium, before separated by high-performance liquid chromatography and analysis with fluorescence detection (long-wave excitation at 480 nm) in the human blood sample. The 3,3'-diaminobenzidine (DAB) is another specific reagent for selenium(IV) detection in the sample as in figure 13. This approach provided a detection limit of 0.15 ng, a standard deviation of 1% at the level of 20 ng (inter-day) and a standard deviation of 3% at the level of 1 ng (within-day).

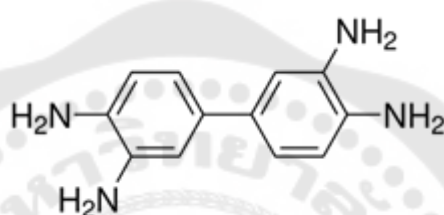


Figure 13 The formula structure of 3,3'-diaminobenzidine (DAB).

In 2002, Niedzielski and coworkers (48) determined selenium(IV) by hydride generation technique combine with atomic absorption spectrometry (HS-AAS). Atomic absorption spectrometry is the analytical tool most commonly used in biological samples to determine total selenium, But atomic absorption spectrometry with conventional flaming atomization has insufficient sample sensitivity. This method shows the concentration detection limit at 0.1 $\mu\text{g/L}$. The most common reducing agent used to obtain Se hydride species is sodium borohydride (NaBH_4). The selenium in the sample could directly be analyzed without any pretreatment sample.

In 2003, Larsen and coworkers (49) were reported applications of inductively coupled plasma-mass spectrometry (ICP-MS) methods coupled with chromatographic separation for selenium analysis in yeast samples. ICP-MS was a popular and powerful technique for determination selenium species at high resolution. The result was 1390 $\mu\text{g/g}$ of total selenium content in the yeast. Selenium determination by ICP-MS is affected by Ar_2 spectral interference, for example. Using reaction-collision cell or high-resolution MS (HRMS) can solve this. ICP-HRMS is a method that is highly sensitive.

In 2001, Stripeikis and coworkers (50) developed a flow injection (FI) separate and pre-concentrated process approach coupled with a spectrometer of electrothermal atomic absorption (graphite furnace). This has been established to evaluate selenite and selenate directly in drinking water. The result showed the detection limit as 10 ng/L, the relative standard deviation (%RSD) ($n=10$) at the 200 ng/L concentration of selenite as 3.5% and selenate as 5.6%, adding regular solutions of selenite and selenate to tap water samples results in a recovery for 97–103% of both species.

In 2014, Feng and coworkers (51) reported a selective fluorescent sample in multivitamin tablets for selenium determination. They synthesized new fluorescent ligand as 2-(2-(2-aminoethylamino)ethyl)-3',6'-bis(ethylamino)-2',7'-dimethyl spiro[isindoline-1,9'-xanthen]-3-one for specific capture with selenium(IV) (Figure 14). The sharp emission of fluorescence was reported in an ethanol solution. The detection limit of Se(IV) was 2.8×10^{-9} mol/L under optimized conditions. The recovery of Se(IV) in four samples ranged from 98% to 103%. This method obtained a small deviation of 2% compared to ICP-AES results.

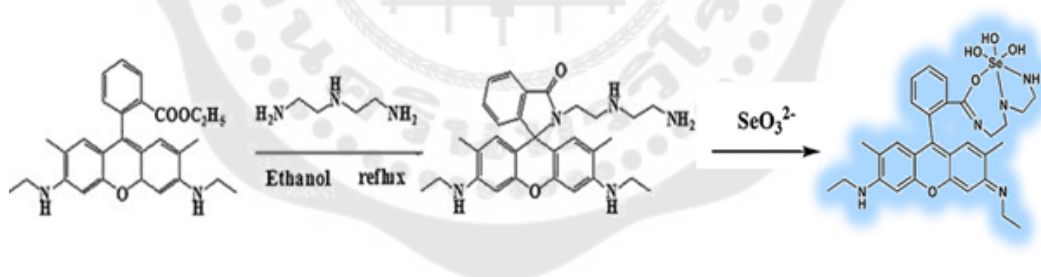


Figure 14 Ligand (2-(2-(2-aminoethylamino)ethyl)-3',6'-bis(ethylamino)-2',7'-dimethylspiro[isindolin-1,9'-xanthen]-3-one) synthesis route.

Source: Feng and coworkers. (51)

In 2013, Liang and coworkers (6) reported the innovation of nanotechnology for determination selenium in the water sample. In this method, the modified surface of silicon nanoparticle with 3,3'-diaminobenzidine (DAB) was prepared as figure 15, and

turn-on fluorescent signal when capturing with selenium(IV). The fluorescent nanoprobe was excited at 420 nm, then emit signals of fluorescence at 530 nm.

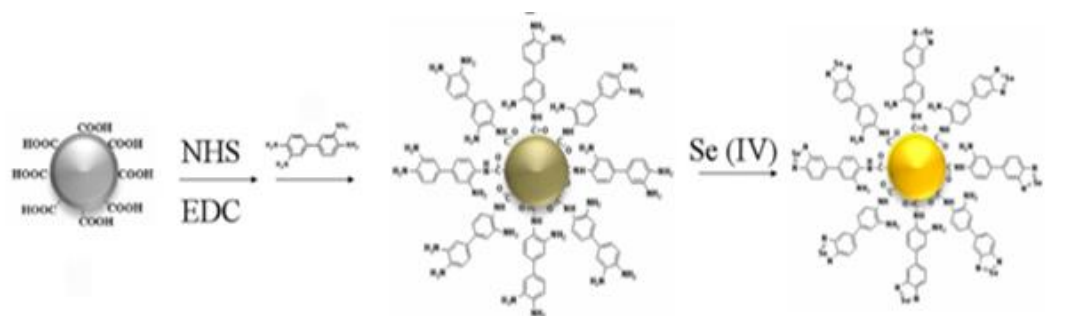


Figure 15 Turn-on fluorescent nanoprobe producing schematic diagram for selenium determination(IV).

Source: Liang and coworkers. (6)

In 2012, Wang and Wu (52) developed highly selective mercury (II) ion fluorescent sensors in applications for live-cell imaging. After synthesis, they predicted the best structure of fluorescent sensors with DFT calculations.

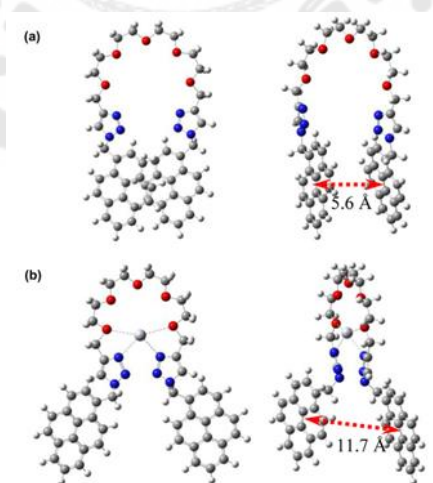


Figure 16 The MS1 (top) and MS1-Hg²⁺ (bottom) DFT-optimized structures; red atom, O; atom blue, N; atom gray, Hg.

Source: Wang and Wu. (52)

In 2016, Mansour (53) studied the electronic structures of the tazarotene-copper complexes both experimentally and theoretically. Calculations using the two-hybrid functional theory of functional density (TD-DFT), B3LYP and CAM-B3LYP were applied to this work. The result was an understanding of the electronic structure.

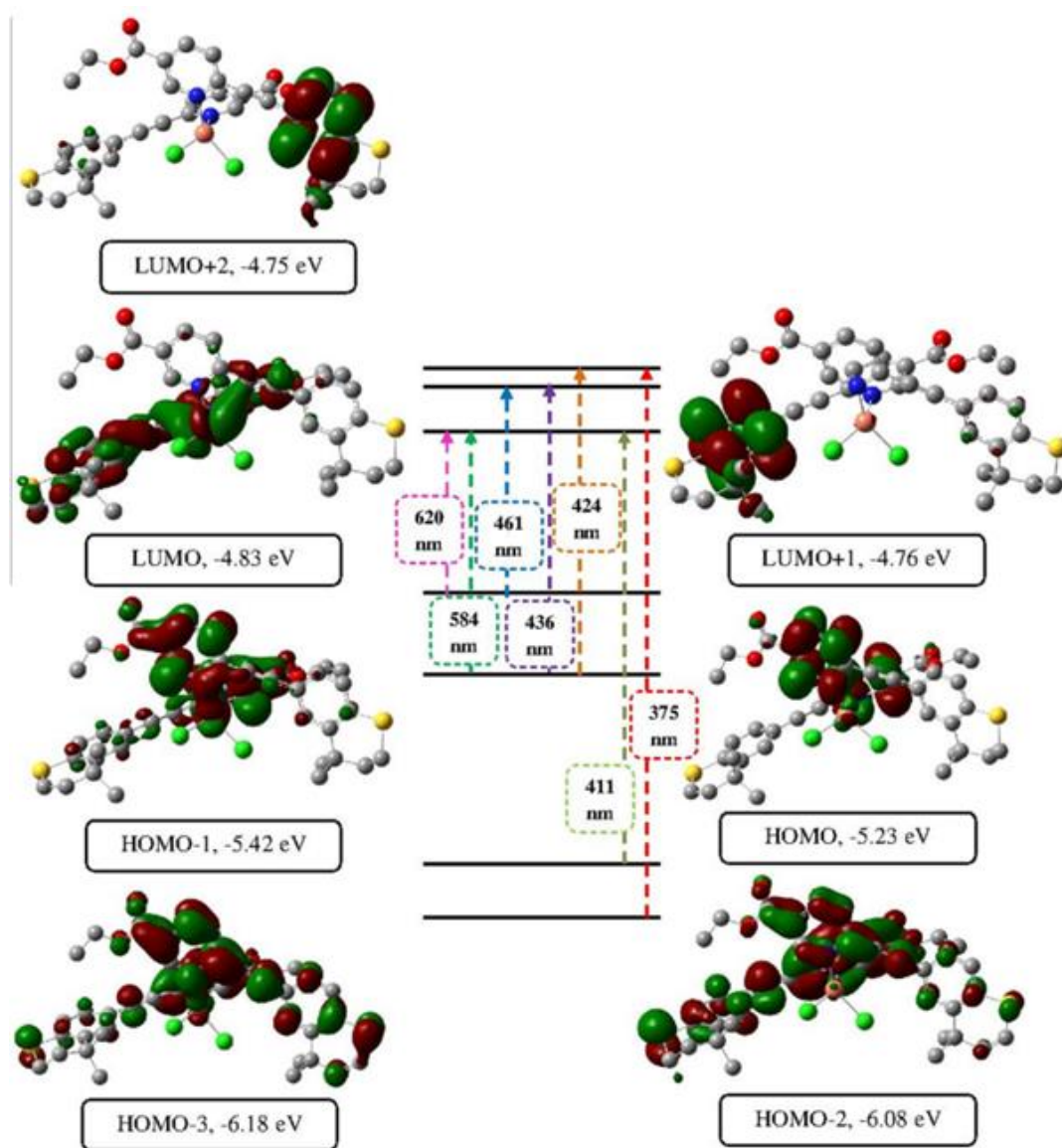


Figure 17 Schematic diagrams of TD-DFT / B3LYP / LANL2DZ calculated transitions of complex electronic absorption.

Source: Mansour. (53)

CHAPTER 3

EXPERIMENTAL

In this chapter, All the experimental techniques, and procedures used to develop fluorescent nanoprobe for quantification of selenium(IV) in the water sample. An instrumentation summary, operating conditions used in analytical measurements and computational chemistry methods of fluorescent nanoprobe also present.

Chemical reagents and Materials

All chemical substances were analytical grade and used without further purification. L-Cysteine 97%, Cadmium dichloride decahydrate ($\text{CdCl}_2 \cdot 10\text{H}_2\text{O}$) 98%, Sodium sulphide nonahydrate ($\text{Na}_2\text{S} \cdot 9\text{H}_2\text{O}$) 98%, 3-Mercaptopropionic acid (3-MPA) 99%, meso-2, 3-dimercaptosuccinic acid (DMSA) 98%, 3,3'-diaminobenzidine (DAB) 99%, 1-ethyl-3-(3-dimethyl aminopropyl) carbodiimide hydrochloride (EDC) 98%, were purchased from Merck® (Germany). Sodium hydroxide (NaOH) 97%, Absolute ethanol (EtOH), N-hydroxysuccinimide (NHS) 98%, were bought from Sigma Aldrich® (USA). N_2 gas 98% were purchased from Pack Air® (Bangkok). Milli-Q water was used in all aqueous experiments unless specified otherwise.

Microcuvette: Spectrosil® micro-cuvette quartz windows (12.5 x 12.5 x 45 mm), 10 mm scale wide, the nominal volume of 0.700 ml (Sterna Cells, Inc., USA) was used for colorimetric analysis. Microfilter: Amicon microcon® YM-30 filters with molecular weight cutoff (Millipore Corporation, Bedford MA, USA) use to remove particulates material from the water sample. Membrane Filter: Nylon filter membranes (0.45 μm pore size, 47 mm i.d.) presented by Agilent Technologies® (Waldbornn, Germany) use to eliminate particulates substance from reagent dilute solution.

Instrumentation

A Fluorescence spectrophotometer was used to record all fluorescence measurements, model: Jasco®, code FP-6200 PC (USA) With slits set at 5.0 nm for both excitation and emission. To scan the spectrum, dilute nanoprobe solutions in the

aqueous medium were placed in 1 cm quartz cuvettes. The solutions absorption spectrum was obtained on a UV-Vis spectrophotometer, model: Shimadzu®, code UV-2401 PC (Yokohama, Japan). Images of the nanoparticles were acquired on a scanning electron microscope (SEM), model: Leo®, (LEO 1450 VP) with energy-dispersive X-ray spectroscopy (EDX) and transmission electron microscope (TEM) (Philips Tecnai 20). The colloidal solution of nanoparticles in water was dropped onto a carbon-coated copper grid with immediate removal of the excess solution. An inductively coupled plasma mass spectrometry (ICP-MS), model: PerkinElmer®, (NexION 300Q) and Atomic absorption spectroscopy Model: PerkinElmer®, (Massachusetts, USA) was used to validate method and compared with synthetic nanoprobles. Analytical Balance, model: Mettler Toledo®, code AB104-S (Zuerich, Switzerland). pH Meter, model: Mettler Toledo®, (Zuerich, Switzerland). Ultrasonic Bath Model: Mettler Toledo®, (Zuerich, Switzerland). Analog Vortex Mixer, model: Scientific Industries®, (New York, USA), (G-560E) with speed control. All-optical tests are carried out under ambient conditions and at room temperature.

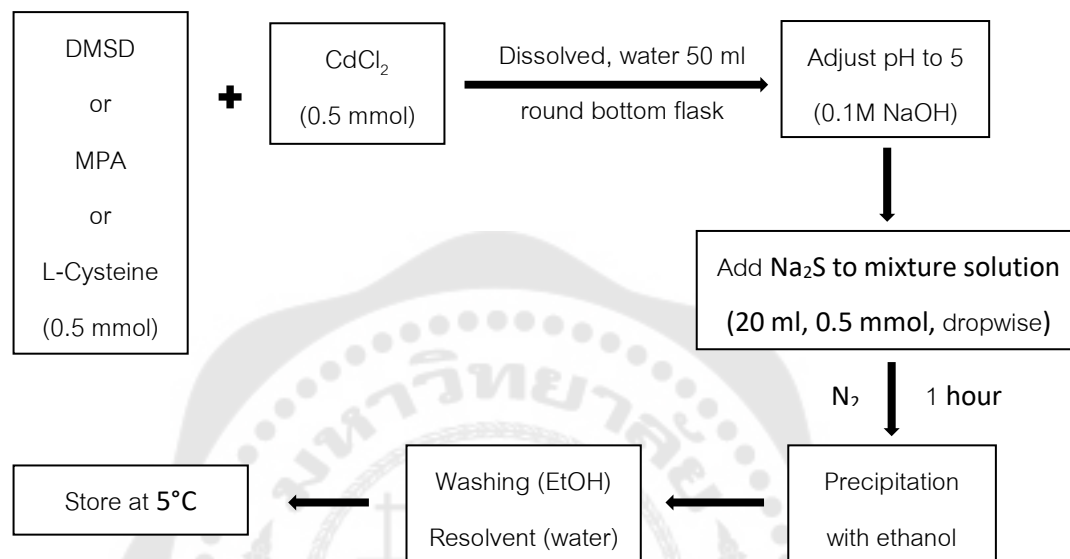
Methods

1. Fabrication of the CdS-Cys-DAB nanoprobles

1.1 Synthesis of CdS Nanoparticle capped with ligand arm

The functionalized three ligands form capped CdS nanoparticle was prepared using the procedures Devi and Koneswaran (54, 55) described, with certain modifications. In a synthesis traditional, 0.5 mmol portions of ligands (DMSD, MPA, and L-Cysteine) and 0.5 mmol of $\text{CdCl}_2 \cdot 10\text{H}_2\text{O}$ were dissolved in 50 ml deionized water and place into a round bottom flask. The pH of the solutions has been changed to increase to 5.0 by adding 0.1 M NaOH drop-wise addition, with constant stirring and magnetic stirrer. Then 0.5 mmol portion of $\text{Na}_2\text{S} \cdot 9\text{H}_2\text{O}$ dissolve in 20 ml of deionized water and the Na_2S solution adds 1 hours of vigorous stirring in the flask. The functionalized ligand capped CdS nanoparticle was treated with three repeated cycles of precipitation by ethanol, washing, and redispersion to remove the contaminants. The luminescent ligand

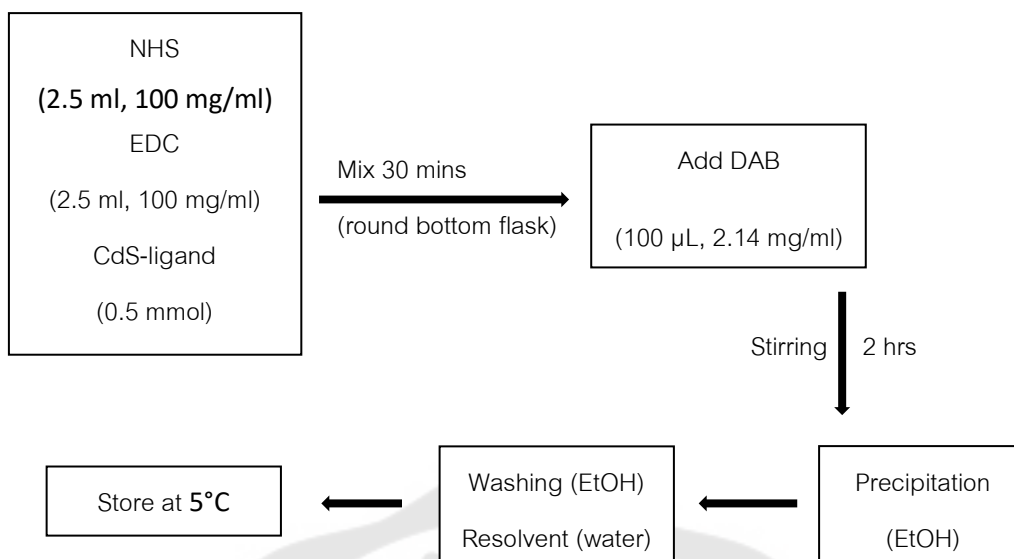
capped CdS nanoparticle was dissolved in double-distilled deionized water and kept at 5°C. Then measure the fluorescent intensity of three luminescent ligands to discuss a successful ligand arm for use in the next step.



1.2 Surface Functionalization of CdS Nanoparticles with DAB Molecules

DAB can immobilize the nanoparticle layer of the ligand-capped CdS by reacting to the cysteine by amine groups with carboxyl groups. Before the reaction, the carboxyl groups are activated. The procedures mentioned have been modified from Liang and coworkers (6).

An aliquot prepares the activation phase by combining 2.5 ml of 100 mg/ml NHS, 2.5 ml of 100 mg/ml EDC and 2.0 ml of a solution of 0.013 mg/ml CdS-ligand nanoparticles (From 1) mixed and left for 30 minutes. The product was then added to 100 μ L of 2.14 mg/ml DAB solution and stirred for 2 hours. The nanoprobes of CdS-ligand-DAB were precipitated by the addition of ethanol and centrifuged for 10 minutes at 10,000 revolutions per minute (rpm). Finally, the filtered precipitate was re-dispersed in deionized water of 100 ml and prepared for further application at 5°C.



1.3 Characterizations of Fluorescent Nanoprobe

The optical properties of fluorescent nanoprobe were recorded UV-visible absorption spectra by spectrophotometer in the range of 250–800 nm. And measurements of photoluminescence by Fluorescence Spectrometer with a wavelength of excitation at 350 nm. These optical measurements are performed by preparing a fluorescent nanoprobe suspension solution in water. In this process, 1 mg of fluorescent nanoprobe is added into 20 ml of water and sonicate (800 W) at ambient temperature for 30 minutes until a homogeneous suspension is formed. This suspension was placed in a quartz cuvette for measurement of optical absorption and photoluminescence. The scanning electron microscope (SEM) and the transmission electron microscope (TEM) evaluated the quality of nanoprobe.

2. Study effect on fluorescent nanoprobe fabrication

2.1 pH effect

The effect of pH on fluorescence nanoprobe to achieve optimal pH on a sensitive selenium fluorescence sensor(IV). The pH influence on this nanoprobe probe was investigated in the range of pH 3 to 11. The optimum pH on the fluorescence intensity of nanoprobe fabrication is measured at room temperature.

2.2 Temperature effect

The effect of temperature on fluorescence nanoprobe to achieve optimum temperature on a sensitive fluorescence sensor for detection selenium(IV). The temperature effect on this investigation in the temperature range between 30°C and 50°C. The optimum temperature on the fluorescence intensity of nanoprobe fabrication is measured at 5 pH.

2.3 Fabrication time

The effect of time used in the production step on fluorescence nanoprobe to achieve the optimum for the detection of selenium(IV) on a sensitive fluorescence sensor. The fabrication time for this investigation from 0 minutes to 240 minutes. The optimum fabrication time on the fluorescence intensity of nanoprobe fabrication is measured at 5 pH and 30°C.

2.4 Ion selectivity test

The effect of ion selectivity on the fluorescence of nanoprobe to obtain a selective fluorescence sensor for selenium(IV). Cation stock solutions (1 ppm) are prepared in deionized water such as Ag(I), As(III), Cd(II), Co(II), Cu(II), Fe(II), Fe(II), Hg(II), Mn(II), Ni(II), Pb(II), Zn(II) which were assessed at room temperature for 5 min at pH 5.0 and 120 minutes. Then the fluorescence intensity was measured in the solution of mixtures between cation and nanoprobe.

2.5 Ion interference test

The effect of ion interference on nanoprobe fluorescence in obtaining the fluorescence detector interference signal for selenium(IV). Cation dilutes solutions (1 ppm) are prepared in deionized water such as Ag and combined with 1 ppm selenium(IV) solution. Then the fluorescence intensity was measured in the solution of mixtures between cation and nanoprobe.

3. Computational study

All the calculations are carried out using the program Gaussian 03. The fluorescent probe's ground state (S_0) geometry was optimized in vacuum using the Density Functional Theory (DFT) approach. The B3LYP functional geometry optimization calculations combined with the 6-31G(d, p) basis-set method for the Ligand-DAB and the Ligand-DAB-Se (complex) geometry optimization were calculations using the B3LYP/6-31G(d, p) gas-phase method. The electronic spectra were determined using the functional B3LYP in combination with the 6-31G(d, p) basis-set using the time-dependent functional density theory (TD-DFT) method. The calculations for the time-dependent functional density theory (TD-DFT) were performed for both the excited state (S_1) and the electronic spectra.

4. Analytical Performances of Development Methods

4.1 Linearity

Selenium (IV) ions detection is performed in ultrapure water for the test fluorescent nanoprobe is dilute in ultrapure water. Working standard selenium(IV) solution at five different concentrations (0.0 to 5.0 ppm) are triplicate by the fluorescent method as described in Sections 1. A five-point calibration curve for selenium (IV) ions is established for a linear least square regression of average fluorescent intensity versus working standard selenium (IV) ion concentrations. The mean intensity was determined from each calibrator's triplicate fluorescent intensity after the blank value is subtracted.

4.2 Precision

The selenium (IV) 5 ppm was treated with the fluorescent method for 10 replications and calculated the relative standard deviation (% RSD) of working standard selenium(IV) solutions using the methods of analysis as defined in Sections 1. Repeatability testing is performed within 1 day, while reproducibility has been conducted in the same method as repeatability testing, but on 5 consecutive days (1, 3, 5, 7, 9 days).

4.3 Limit of Detection

Various methods for evaluating the detection limit are appropriate on the bases of the recommendation of the International Conference on Harmonization (ICH). The signal-to-noise ratio is calculated by comparing measured signals from samples with known low analyte concentrations with those from blank samples and by evaluating the minimum concentration at which the analyte can be detected reliably. To estimate the detection limit, a signal-to-noise ratio of 3 or 2:1 is generally considered appropriate. In this case, a water sample with known spiking concentrations of standard selenium solutions(IV) is evaluated, the detection limit is a determination can be expressed as:

$$\text{LOD} = \frac{3.3 \sigma}{S} \quad \text{----- [5]}$$

where σ is the standard deviation of the response

S is the slope of the calibration curve

The slope S can be estimated using the analyte's calibration curve. For this method, the σ estimate can be defined as triplicating the standard deviation (SD) of the blank sample mean ($n=10$).

4.4 Recovery Studies

Water samples are ultrafilter using the same condition. The ultrafiltrate (5 ml) is then spiked with the 5 ppm selenium(IV) standard solutions. The percentage of recovery calculate by comparing the mean fluorescent intensity obtain for the spiked sample with those obtained for direct measurement of working standard solutions ($n=5$).

4.5 Statistical Analysis

All statistical analysis was performed using the MS-Excel statistics data values system are express as the mean \pm the standard deviation (SD) unless otherwise states.

5. Application on Determination of selenium in samples

Vegetable samples were brought from Foodland Supermarket in Bangkok, Thailand. All of the samples were peeled and washed with deionized water to remove impurities and chopped into small pieces. Then 50 g of samples were digested with 50 ml HNO_3 (65%) and 15 ml H_2O_2 (30%) on a hotplate for 120 mins. After digestion, the residues samples were filtered out and the solution samples were collected and stored at 5° C.

Selenium(IV) was determined using the nanoprobe developed in the sample solution. A 1.0 ml aliquot of CdS-Cys-DAB added to 1.0 ml of sample solutions and various Se(IV) concentrations solution (final concentration, 0.0 to 5.0 ppm). Then the pH was adjusted to 5 (0.1M NaOH) and vortexed for 5 mins. The mixture solution was filtered using a 50 nm porous membrane and then measured with a fluorescence spectrometer. In order to obtain analyte concentration, the resulting intensity was compared with the standard calibration curve.

CHAPTER 4

Results and Discussion

In this research, we focus on the development of the synthesized CdS nanoparticles and surface functionalization of these nanoparticles using DAB molecules. The outline of the study is as follows:

1. Fabrication of the CdS-Cys-DAB nanoprobe
 - 1.1 Synthesis of CdS Nanoparticle capped with ligand arm
 - 1.2 Surface Functionalization of CdS Nanoparticles with DAB Molecules
 - 1.3 Characterizations of CdS-Cys-DAB Nanoprobe
2. Study effect on fluorescent nanoprobe fabrication
 - 2.1 pH effect condition
 - 2.2 Temperature effect condition
 - 2.3 Fabrication time
 - 2.3 Ion selectivity test
 - 2.4 Ion interference test
3. Computations study
4. Analytical performance of CdS-Cys-DAB nanoprobe
5. Application on Determination of selenium(IV) in samples

1. Fabrication of the CdS-Cys-DAB nanoprobe

An important step in making the selective fluorescent nanoprobe for selenium is to choose the appropriate selenium-induced fluorescence molecule which generates fluorescence signal when bound with selenium contained in the sample. Previously, 3,3-diaminobenzidine (DAB) was used for selenium detection (56). That study suggested that DAB selectively showed the high in response to selenium ion. In this research, DAB has been selected as a molecule for the selective selenium reagent to make the nanoprobe.

1.1 Synthesis of CdS Nanoparticle capped with ligand arm

The CdS core nanoparticle was synthesized by bottom-up colloidal crystal assembly. In Figure 18A, An approach from the bottom-up, Where a molecular precursor is decomposed to produce metal atoms that nucleate and develop into monodispersed colloids. However, the top-down approach, where large drops of metal are broken into smaller pieces and then transformed by shear forces into uniform droplets by a mechanism similar to conventional emulsification. Mostly two reaction mechanisms (Figure 19) are involved in the synthesis of CdS nanoparticles,

1. Ostwald's ripening
2. Particle agglomeration.

In particular, crystal growth during in-situ precursor heating follows a significant path of Ostwald ripening in which surface energy decreases when large particles are produced by the use of smaller particles. However, the ripening of nanoparticles is driven by numerous criteria such as precursor, temperature, species reactivity, etc.

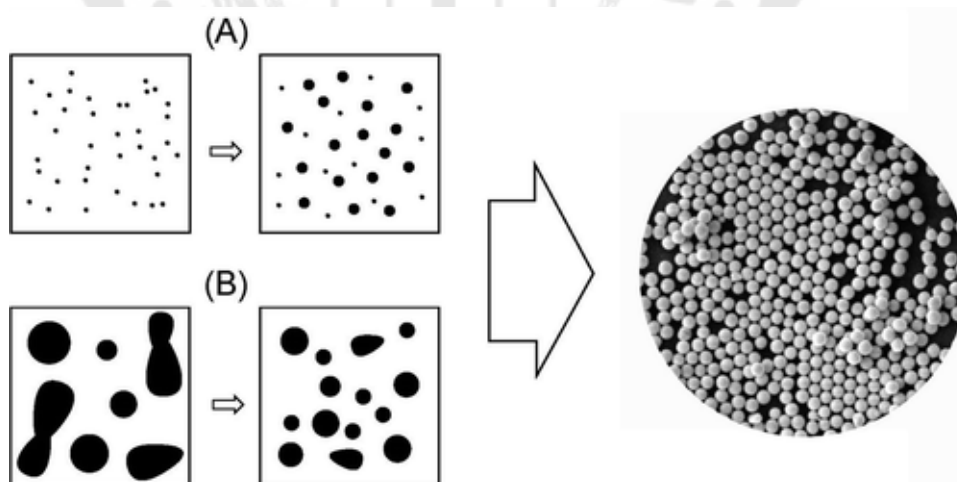


Figure 18 Schematic diagram of two distinct solutions to monodispersed spherical metal colloids, (A) bottom-up and (B) Top-down methods.

Source: Yuliang Wang and Younan Xia (57)

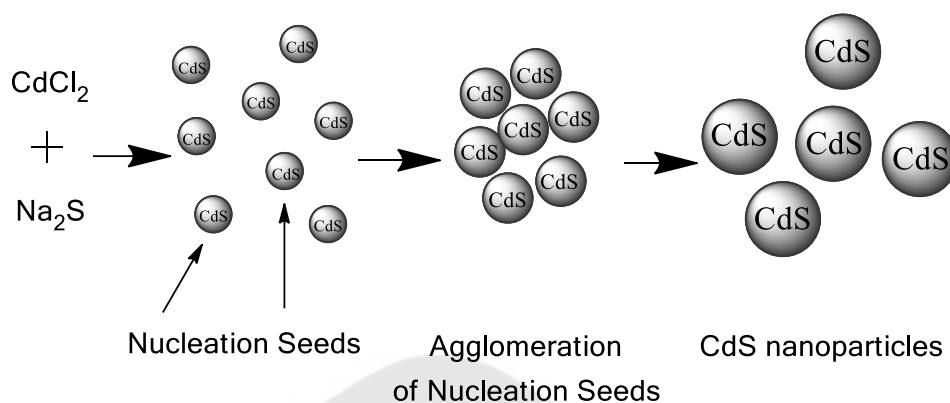


Figure 19 Growth mechanism of CdS nanoparticles.

Source: Adapted from Devi. (54)

In this study, the colloidal bottom-up synthesized according to the method previously reported (54). Figure 20 represents CdS nanoparticle illustrations capped with three types of thiol-ligand arms. Meso-2, 3-dimercaptosuccinic acid (DMSA), 3-mercaptopropionic acid (MPA), and L-cysteine (Cys) were the ligands used in this study. Therefore, the thiol-ligand group has easier disulfide-bonded with CdS core nanoparticle. The precursor solution gradually turned from light to yellow-green (Appendix section). The chemical reaction is as follows:



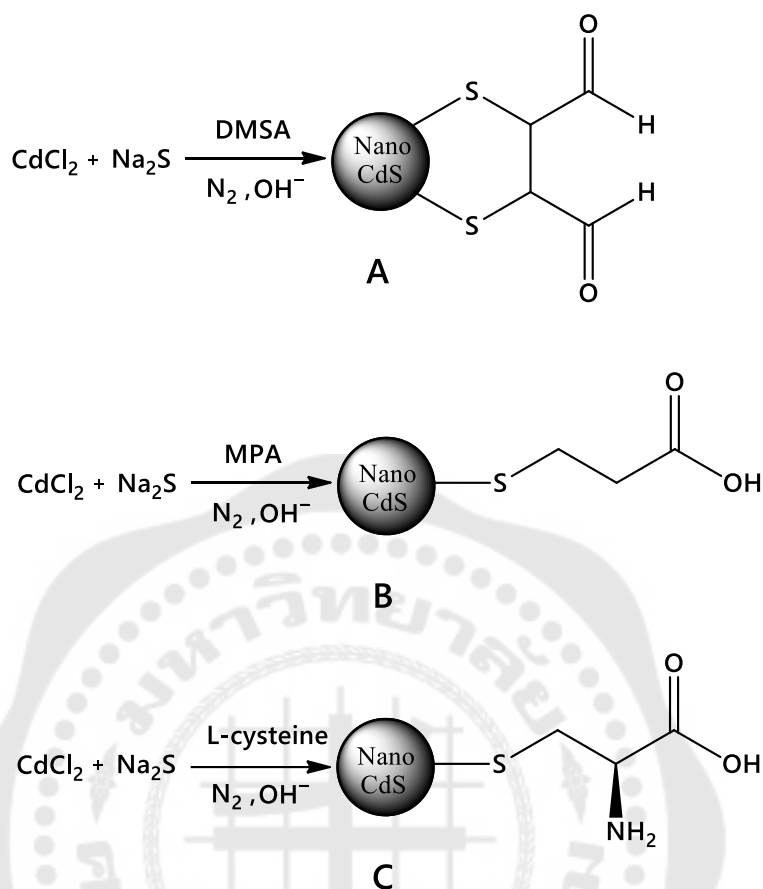


Figure 20 Illustrates of CdS nanoparticle capped with 3 types of ligand arms, (A) capped with DMSA, (B) capped with MPA, (C) capped with L-cysteine.

The results of fluorescence intensity the CdS nanoparticle capped with a ligand. As shown in Table 3. The ligands of Meso-2, 3-dimercaptosuccinic acid (DMSA) and 3-mercaptopropionic acid (3-MPA) had a higher intensity of fluorescence than L-cysteine. However, both Meso-2, 3-dimercaptosuccinic acid and 3-mercaptopropionic acid are more toxic, carcinogenic sustain and expensive. Therefore, L-cysteine becomes a good choice to use for the ligand arm of CdS nanoparticle. Although, L-cysteine was a little lower fluorescence intensity than 2 ligands above it still strong fluorescence intensity. Moreover, L-cysteine is low cost, non-toxic and the good of the environment.

Table 3 Fluorescent intensity of ligands arm capped.

Ligand capped.	Fluorescent Intensity (LU)
DMSA	194
MPA	201
L-Cysteine	183

1.2 Surface Functionalization of CdS Nanoparticles with DAB Molecules

After selecting the matrix and sample molecules, immobilizing the sample molecules on the surface of the CdS-L-cysteine nanoparticles is the essential step to make the nanoprobes. A molecule of 3,3'-diaminobenzidine (DAB) has two sets of different sides of amine groups (Figure 21), This makes it possible to immobilize DAB to the surface of the nanoparticles. Carboxyl groups can interact easily with amine groups on the base of knowledge of chemical reactions. Therefore, the next key step in the manufacture of fabrication nanoprobes will be to introduce carboxyl groups to the surface of CdS-Cys nanoparticles.

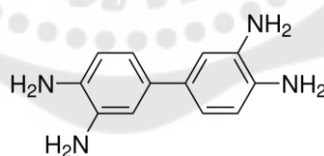


Figure 21 Structure of 3,3'-diaminobenzidine (DAB) molecule

The activation of carboxyl groups on nanoparticles is required to initiate the reaction of carboxyl groups on the surface of the nanoparticles with amine groups on DAB molecules.

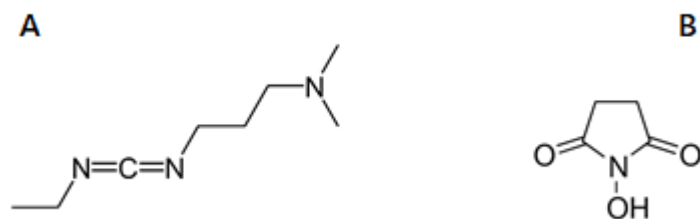


Figure 22 Structure of (A) 1-ethyl-3-(3-dimethyl aminopropyl) carbodiimide hydrochloride (EDC) and (B) N-hydroxysuccinimide (NHS) molecule

For this activation, a 1-ethyl-3-(3-dimethyl aminopropyl) carbodiimide hydrochloride (EDC) (Figure 22A) was selected as EDC-Crosslink may form intermediate (unstable) *o*-acylisourea with carboxyl groups on nanoparticles surface. NHS (Figure 22B) was subsequently used to increase the coupling efficiency of carboxyl groups with amine groups through the formation of active ester intermediates, More stable than *o*-acylisourea intermediates. The crosslinking reaction scheme of Sulfo-NHS plus EDC (carbodiimide) is as shown in figure 23.

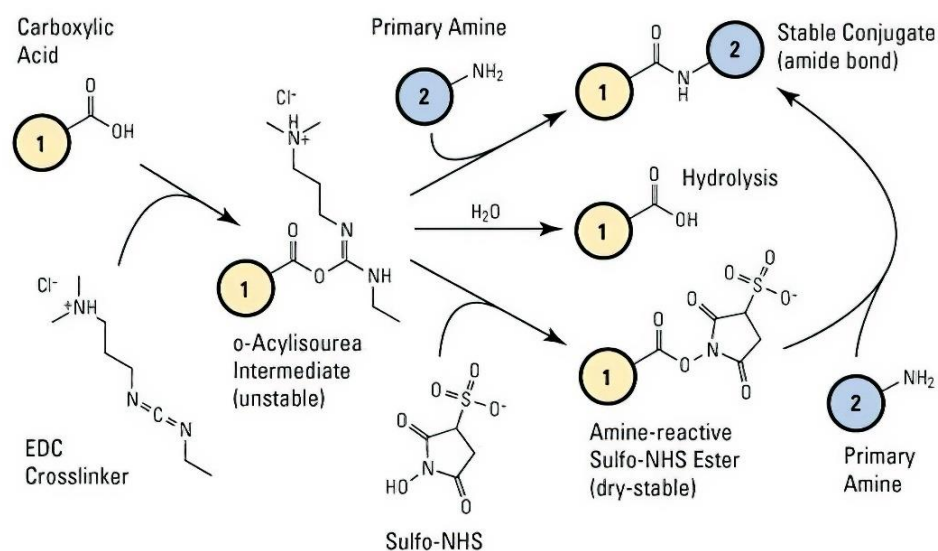


Figure 23 Scheme of crosslinking reaction of Sulfo-NHS and EDC (carbodiimide)

Source: Thermofisher catalog number: 22980 (58)

DAB (primary amine) then reacted with the intermediates and substituted the EDC and NHS. When properly controlled the ratio of nanoparticles to DAB molecules, one amine pair group on a DAB molecule can connect to the surface of the nanoparticles. Therefore, the nanoprobe of selenium have been produced (Figure 24A). The other group of amine pairs on the DAB molecule can then bind to target selenium and create a fluorescent complex (Figure 24B).

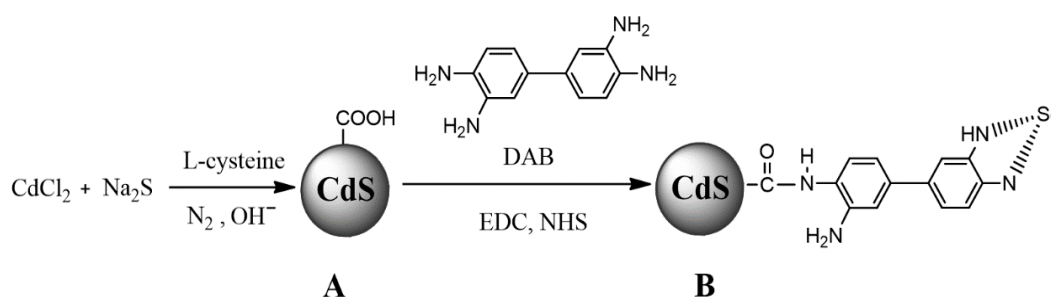


Figure 24 Schematic diagram shows the fabrication of the CdS-Cys-DAB nanoprobe used to determine selenium(IV). (A) CdS-Cys nanoparticle. (B) DAB modified on CdS-Cys nanoparticle for selenium measurement.

Source: Adapted from Devi. (54)

1.3 Characterizations of CdS-Cys-DAB Nanoprobe.

A scanning electron microscope (SEM) and transmission electron microscope (TEM) characterized the morphology of the nanoprobe. First, The CdS-Cys nanoparticles' SEM and TEM images have been taken. The results showed that the average diameter of the CdS-Cys nanoparticles was 20 nm (Figure 25A) and the shell layer of cysteine capped on CdS core nanoparticles was observed (Figure 25B). After the DAB molecules were immobilized on the nanoparticle, the size and shape of the nanoprobe were significantly changed and the modified layer of DAB was fixed on the core surface (Figure 25C), there was an average particle size of 50 nm. The fluorescent spectra of the nanoprobe are shown in Figure 26. A strong emission peak of CdS-Cys-DAB functionalized nanoprobe was observed at 390 nm (Figure 26A) compared with

the emission peak of CdS-Cys nanoparticles (Figure 26B) when the excitation wavelength was 280 nm.

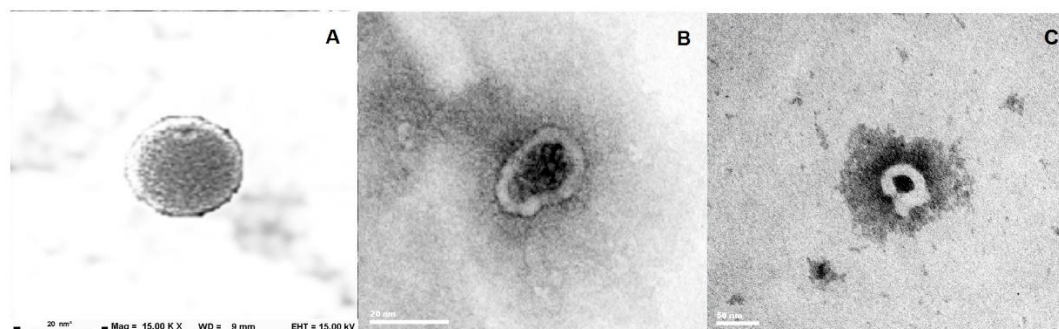


Figure 25 CdS-Cys nanoparticles SEM and TEM images (A and B). TEM images of nanoprobe (C) operated by CdS-Cys-DAB.

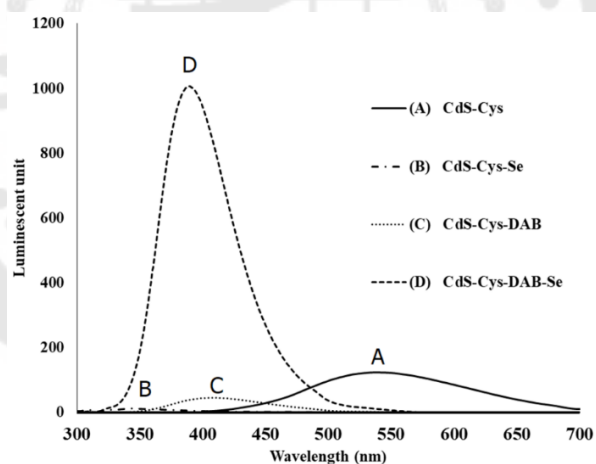


Figure 26 (A) CdS-L-cysteine nanoparticles fluorescent emission spectrum, (B) CdS-Cys nanoparticles with the presence of Selenium(IV), (C) CdS-Cys-DAB nanoprobe and (D) CdS-Cys-DAB nanoprobe in the presence of Se(IV) present. The excitation wavelength was set at 280 nm.

Energy-dispersive X-ray spectroscopy (EDS) is a standard method for elementary composition detection and quantification in a very small material sample (including a few cubic micrometers). In a properly equipped SEM, the electron beam

excites the atoms on the surface. Emission of unique X-ray wavelengths indicative of the element's atomic structure. Those X-ray emissions can be analyzed by an energy-dispersive detector (a solid-state device that discriminates between X-ray energies). Suitable elements are assigned, resulting in the arrangement of the atoms on the surface of the sample. This technique is called energy-dispersive X-ray spectroscopy (EDS) and can be used to analyze the surface composition of a sample. The energy-dispersive X-ray spectroscopy of CdS-Cys-DAB functionalized nanoprobe observed atom composition as C = 41.98%, N = 4.20%, O = 17.46%, S = 20.10% and Cd = 16.26% by atomic percentage. When this functionalized nanoprobe captured selenium(IV) (5 ppm). The energy-dispersive X-ray spectroscopy of CdS-Cys-DAB functionalized nanoprobe observed atom composition change as C = 36.32%, N = 5.22%, O = 11.54%, S = 21.46% and Cd = 15.78% and Se = 9.67%. The illustration of CdS-Cys-DAB and CdS-Cys-DAB captured with selenium(IV) EDS spectrum are shown in Figure 27A and 27B, respectively.

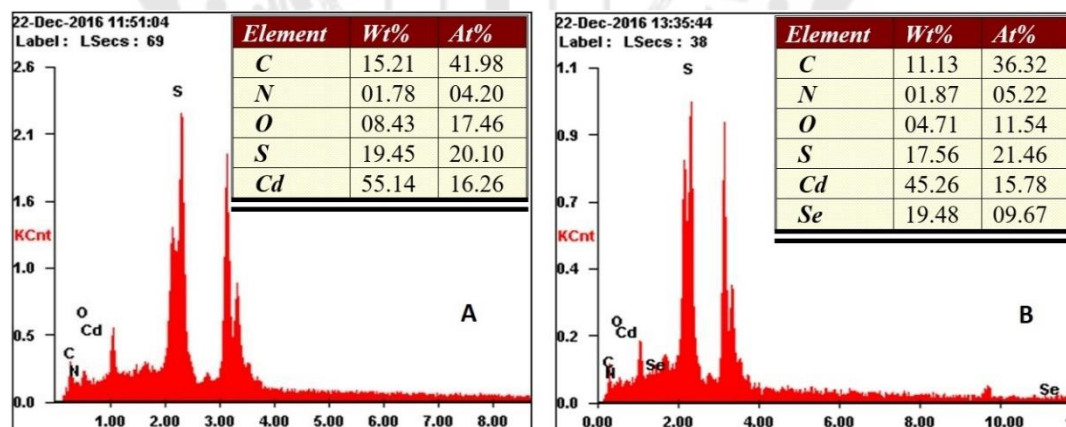


Figure 27 The illustration of the EDS spectrum as 1. (A) bare nanoprobe and 2. (B) captured with Selenium(IV)

2. Study effect on fluorescent nanoprobe fabrication

Selenium(IV) determination using DAB molecules was previously studied (59). These studies showed that several experimental conditions had a significant impact on CdS-Cys-DAB nanoprobe-Se complex fluorescence signals; In particular, fluorescence measurement was significantly affected by pH and temperature.

2.1 pH effect condition

The CdS-Cys-DAB nanoprobe-Se complex's fluorescence property is sensitive to the solution's pH value. Table 4 shows when higher fluorescence signals are given by pH solution at acidic media. However, high acidity will cause the CdS-Cys-DAB nanoprobe to be aggregated. In addition, the amide bonds between the nanoparticles and DAB are broken at high acidity, thereby damaging the nanoprobe. It is important to determine the optimum pH for selenium determination using the nanoprobe CdS-Cys-DAB. A series of solutions with different pH values have been tested for selenium detection using nanoprobe was shown in Table 4.

Table 4 Table of the solution pH effect on the fluorescence intensity of the CdS-Cys-DAB nanoprobe-Se(IV) complex.

pH Constant	Fluorescent intensity (Luminescent unit)
3	Not Detected
4	Not Detected
5	236
6	182
7	147
8	132
9	121
10	118
11	112
12	Not Detected

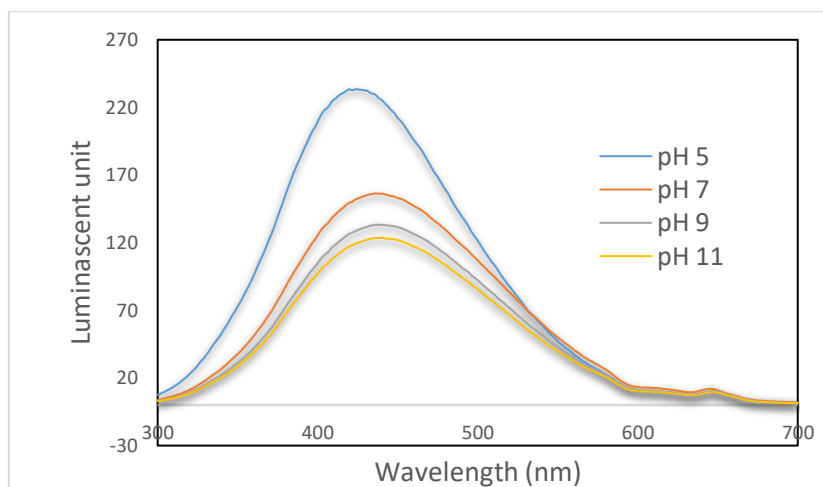


Figure 28 The solution pH effect on the fluorescence spectrum of the CdS-Cys-DAB nanoprobe-Se(IV) complex.

Figure 28 was apparent that the intensity of the fluorescence decreased as the pH increased. In the meantime, it was possible to observe obvious precipitation of CdS-Cys-DAB nanoprobe when the solution pH was below 4. However, the fluorescence intensity remained constant in the range of pH 4 to 5. The pH at 5 is therefore suitable for the condition of nanoprobe in manufacturing. A pH 5 value was used in this work.

2.2 Temperature effect condition

Because temperature has an obvious effect on fluorescence properties. The temperature of the CdS-Cys-DAB nanoprobe solution was monitored by a water bath in the range of 30°C to 70°C to test the fluorescent intensity change with temperature (excitation wavelength was set at 280 nm). As shown in Table 5, CdS-Cys-DAB nanoprobe fluorescence decreases with temperature rise and fall significantly with higher temperatures. The initial yellow-green transparent solution was changed to turbid (Figure 44, Appendix). This could be an effect of the shrinking state (60) Due to the increased hydrophobic effect of the CdS-Cys-DAB nanoprobe at high temperatures and reduced overall fluorescence strength of the CdS-Cys-DAB nanoprobe. In addition, the shrinking state of the nanoprobe CdS-Cys-DAB would also greatly increase its

absorption, refraction and light dispersion, transforming (61) it into a strong light dispersing center and thus increasing its total fluorescence (more than 50 ° C). The lower temperature is therefore ideal for processing nanoprobe. Figure 29 showed the highest level of emissions at 30 ° C. The temperature value at 30 ° C has also been used in this work.

Table 5 Table of the solution temperature effect on the fluorescence intensity of the CdS-Cys-DAB nanoprobe-Se(IV) complex.

Temperature (Celsius)	Fluorescent intensity (Luminascent unit)
30	234
40	97
50	29
60	Not Detected
70	Not Detected

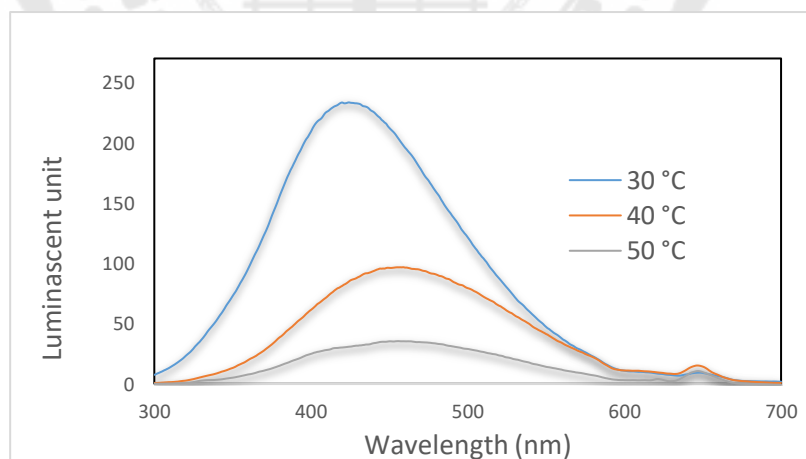


Figure 29 The solution pH effect on the temperature spectrum of the CdS-Cys-DAB nanoprobe-Se(IV) complex.

2.3 Fabrication time

Another test was rendered by systematically increasing the synthesis time from 0 minutes to 240 minutes. Figure 30 indicates the fluorescent intensity depends on the time of CdS-Cys-DAB nanoprobe synthesis. The effect has been observed as strength increases as synthesis time increases. Because of the synthesis rate arising from early (0 minutes to 120 minutes) conversion of the common precursor into nanoparticle material. But the fluorescent intensity will not increase significantly if it increases the synthesis time more than 120 minutes. Due to the loss of free precursor for producing nanoparticles, the reaction rate decreases. Thus the optimal nanoprobe synthesis of CdS-Cys-DAB was set at 120 minutes.

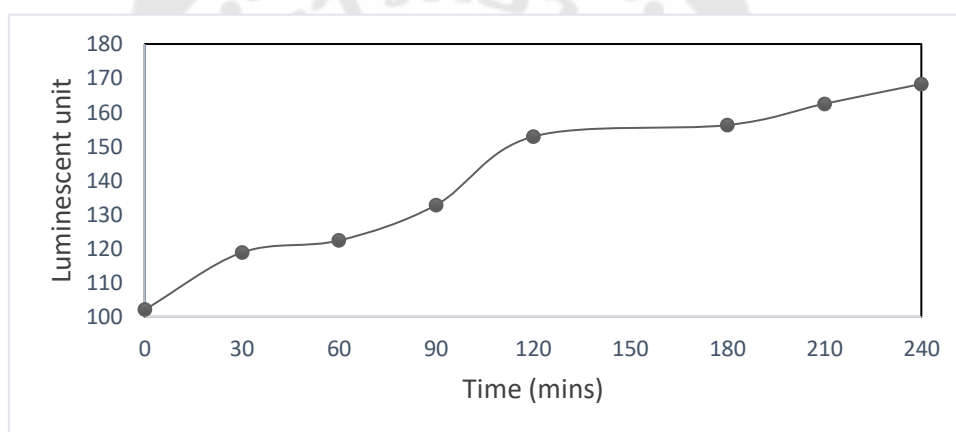


Figure 30 The fluorescent intensity dependence for CdS-Cys-DAB synthesis time.

2.4 Ion selectivity effect

In order to evaluate the selectivity of CdS-Cys-DAB nanoprobe against different metal ions, nanoprobe fluorescence spectra are measured at 1 ppm in the presence of several metal cations such as Ag(I), Cd(II), Co(II), Cu(II), Fe(II), Fe(III), Hg(II), Mn(II), Ni(II), Pb(II) and Zn(II). The solution was thoroughly mixed and added to the nanoprobe solution for CdS-Cys-DAB. Figure 31 showed the effect of metal ions on nanoprobe fluorescence in solution. Apparently, the fluorescence signal of the selenium nanoprobe was 14 times higher than another cation.

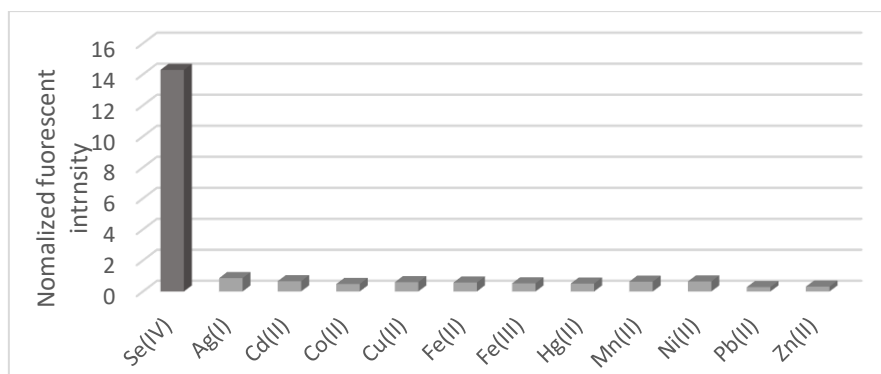


Figure 31 Comparison of the CdS-Cys-DAB nanoprobes responses to the selenium ion for common metal ions.

2.5 Ion interference effect

The effect on the fluorescence of CdS-Cys-DAB nanoprobes of different coexisting ions was analyzed by mixing a concentration of 1 ppm Se(VI) ion solution and interfering with ions at a concentration as shown in Table 6. The solution was thoroughly mixed and added to the nanoprobes solution for CdS-Cys-DAB. CdS-Cys-DAB nanoprobes fluorescence spectra have been recorded in the presence of interfering ions and fluorescence intensity changes are shown in Figure 31. The relative standard deviation of the solution containing 1 ppm Se(IV) for five replicate measurements was estimated at 1.66%. Therefore, error-causing ions prefer less impact on this probe from interferents.

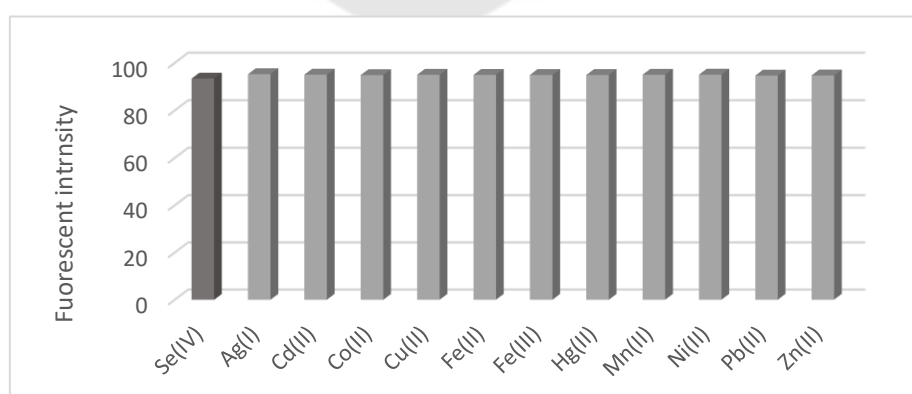


Figure 32 Effect of foreign interference ions on functional CdS-Cys-DAB nanoprobes fluorescence intensity.

Table 6 the error percentage of the ion interference effect study.

Potential interferent	Change of fluorescence intensity (%)
Ag(I)	±1.99
Cd(II)	±1.77
Co(II)	±1.58
Cu(II)	±1.71
Fe(II)	±1.68
Fe(III)	±1.62
Hg(II)	±1.61
Mn(II)	±1.74
Ni(II)	±1.76
Pb(II)	±1.36
Zn(II)	±1.40

3. Computations study

A B3LYP/6-31G(d, p) method with a Gaussian 03 package was used to gain insight into the electronic properties of Cys-DAB-Se complex, time-dependent density functional theory (TD-DFT) calculations. For Cys-DAB-Se complex, molecular orbitals in the ground state are shown in figure 33. Calculations for TD-DFT revealed two potent transitions at 316.45 nm and 362.89 nm = 0.2490 and 0.0455, respectively. which correspond to HOMO-1 \rightarrow LUMO+1 and HOMO \rightarrow LUMO respectively are presented in figure 34. The transition band at a higher wavelength may be assigned to an intramolecular charge transfer (ICT) band due to charge transfer from the Cys-DAB-Se complex donor moiety (HOMO) to the Cys-DAB-Se complex (LUMO). The energies of the HOMO and LUMO levels and the bandgap of the Cys-DAB-Se complex were found to be -3.91, -3.41 and 0.5 eV. The comparison of electronic properties is both

experimental and calculation, Table 7 shown the excitation wavelength Cys-DAB-Se's complex form calculation and experiment was 316.45 nm and 280 nm, respectively.

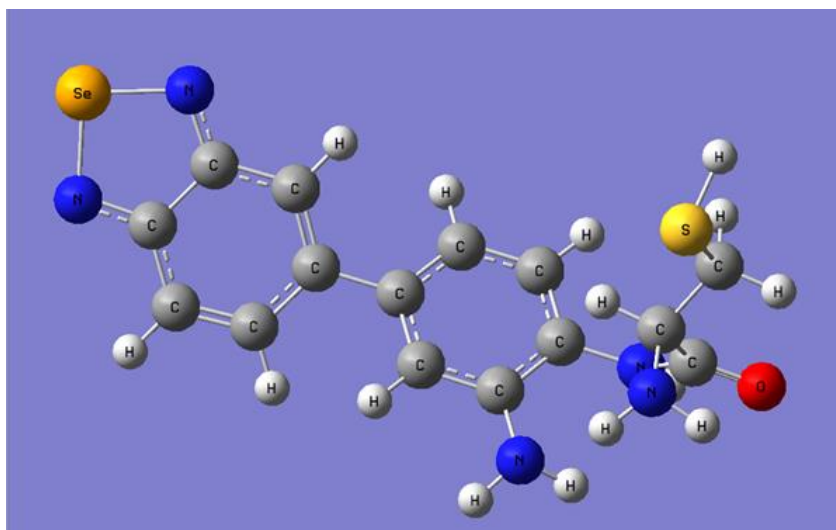


Figure 33 The optimized structure of Cys-DAB-Se complex.

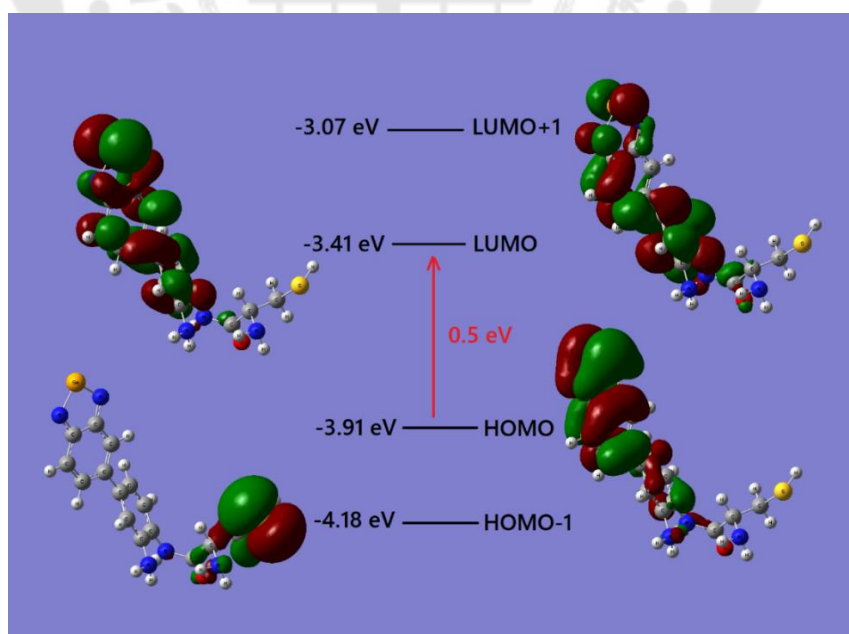


Figure 34 The LUMO and HOMO frontier molecular orbital amplitude plots of this probe by Gaussian process B3LYP/6-31G(d, p).

Table 7 Excitation wavelength forms calculation and experimental methods.

Methods	Excitation wavelength (nm)
Calculation	316.44
Experimental	280.00

4. Analytical performance of CdS-Cys-DAB nanoprobe

In an aqueous solution, the fluorescence emission at 390 nm with an excitation of 280 nm was selected to determine selenium(IV). The level of fluorescence intensity was proportional to the level of selenium(IV). Figure 35 showed this detection's linear regression plot was 0.0 ppm to 5.0 ppm with $y = 0.0901x - 0.0334$, $R^2 = 0.9647$. The detection limit (LOD) and the quality limit (LOQ) was 0.12 ppm and 0.38 ppm. Respectively.

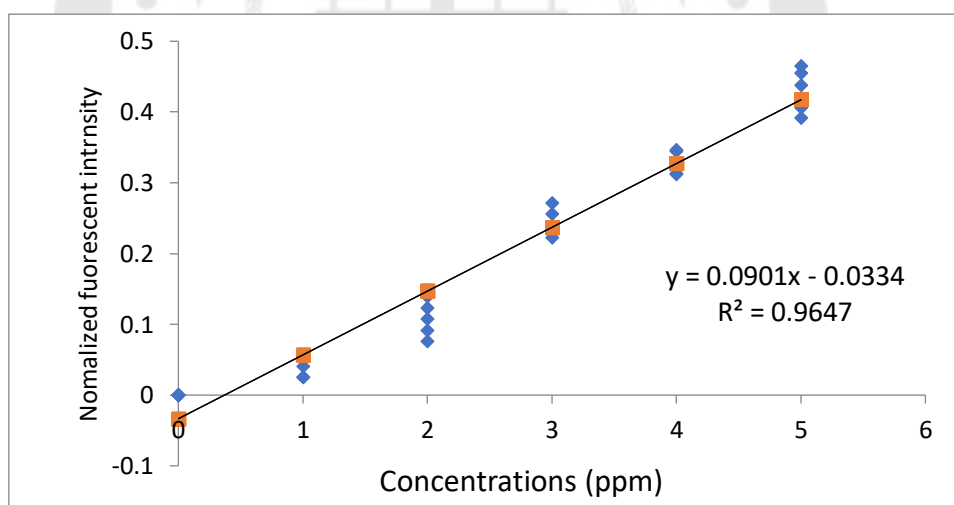


Figure 35 The linear regression range of CdS-Cys-DAB nanoprobe

The relative standard deviation for the comparison process was 3.2 percent (five tests of replication). Similar to the ICP-MS method for selenium detection, both the linear range and the detection limit are better than the AAS method. These nanoprobe are being used for the in situ detection of selenium. The analytical performance of CdS-Cys-DAB nanoprobe compared with ICP-MS and AAS shown in Table 8.

Table 8 The analytical performance of CdS-Cys-DAB nanoprobe

Parameter	Analytical Method		
	AAS ^a	ICP-MS ^b	This study
Instrument cost	High	Very-high	Low
Added (ppm)	5.000	5.000	5.000
Found (ppm), (\pm SD, n = 5)	4.458(\pm 4.4)	4.880(\pm 2.2)	4.565(\pm 2.9)
%Recovery, (\pm SD, n = 5)	89.16(\pm 3.7)	97.6 (\pm 2.6)	91.3(\pm 2.4)
Linearity range (ppm)	2.0 – 80.0	0.1 – 100.0	0.50 – 100.0
Detection limit (ppm)	0.5	0.1	0.2
RSD% Intra-day (n=10)	5.6%	1.3%	3.2%
RSD% Inter-day (n=10)	8.1%	2.4%	4.5%

^a AA condition air/C₂H₂ used for a gas carrier, resonance line at 196.0 nm and 2.0 nm slit width.

^b ICP conditions, sample uptake rate 0.25 mL/min, RF power 1500 W, collision mode He = 4 mL/min and reaction mode CH₄ = 0.65 mL/min.

5. Application on Determination of selenium(IV) in samples

The proposed method of selenium(IV) measurement was applied in the vegetable of the Allium species sample. The sample was treated and determination by the proposed method. Table 9 showed the selenium content found in of Allium species. In the vegetable sample, the results observe selenium levels in the garlic sample was about higher than in another sample. The selenium levels in the vegetable sample were approximate 0.93 μ g. But a selenium level in all Allium species samples was still lower than a selenium level limit (4.0 μ g) for healthy people (62).

Table 9 Results of selenium determination (n = 3) in raw vegetables

Vegetable sample	Selenium Content (μg)		
	AAS ^a	USDA ^b	This study
Onion (<i>Allium cepa</i>)	0.56	0.50	0.45
Garlic (<i>Allium sativum</i>)	1.49	1.40	1.41
Scallion (<i>Allium allioideae</i>)	0.95	1.00	0.96
Shallot (<i>Allium ascalonicum</i>)	1.05	1.00	0.92

^a AA condition was air/C₂H₂ used for a gas carrier, resonance line at 196.0 nm and 2.0 nm slit width.

^b USDA Agricultural Research Service (63)



CHAPTER 5

Conclusions and Recommendation

The main objective of this dissertation was to use synthesized water-soluble functionalized CdS-Cys-DAB nanoprobe was synthesized for use as a luminescent probe for selenium(IV) detection. This nanoprobe is focused on the enhancement of the fluorescence of selenium ions, which interacts with CdS-Cys-DAB nanoprobe.

The CdS capped with thiol ligand arm was synthesized by bottom-up colloidal crystal assembly. L-cysteine was the best choice of thiol ligand ligands link for nanoprobe arm. Because CdS-Cys capped with L-cysteine was strong fluorescence intensity, low cost, non-toxic and the good of the environment. After synthesized core nanoprobe, the DAB was immobilized to the CdS-L-cysteine for specific capture to selenium(IV). The reaction used EDC and NHS to activate L-cysteine to immobilization DAB. After synthesized, the morphology used to confirm the fabrication CdS-Cys-DAB nanoprobe. The SEM and TEM images observed this probe in nanoscale, average particle size at 50 nm.

This CdS-Cys-DAB nanoprobe has some effect on pH and temperature in the synthesis step. At pH, lower acidic media give higher fluorescence signals. But, when more acidic. The CdS-Cys-DAB nanoprobe lead to aggregation of nanoprobe and amine bond broke form DAB linker. Meanwhile, in higher pH, the CdS-Cys-DAB has the effect of precipitation. Therefore, the pH at 5 is suitable for fabrication nanoprobe condition. With temperature rise, the fluorescence of the CdS-Cys-DAB nanoprobe decreases and drops sharply when the temperature is higher. This can be attributed to the shrinking state caused by the increased hydrophobic effect of the nanoprobe CdS-Cys-DAB at high temperatures. Thus, the lower temperature is suitable for fabrication nanoprobe condition. In this work, a value of temperature at 30°C. This nanoprobe has high selectivity of Se(IV) over 14 times when compared with other metal. The percentage of ions causing errors in CdS-Cys-DAB nanoprobe was estimated at 1.66%. Thus, ions causing errors prefer less effect from interferents on this probe.

The TD-DFT calculations of these nanoprobe were used with a Gaussian 03 package using a B3LYP/6-31G(d, p) method. The result was two strong transitions with an oscillator strength at 316.45 nm and 362.89 nm from HOMO-1 \rightarrow LUMO+1 and HOMO \rightarrow LUMO, respectively. The HOMO and LUMO levels of the Cys-DAB-Se complex's bandgap energies were found to be 0.5 eV. when comparison electronic properties form calculation and experimental. The excitation wavelength of the Cys-DAB-Se complex form calculation and experiment was 316.45 nm and 280 nm, respectively.

After a study of the analytical performance of CdS-Cys-DAB nanoprobe. This nanoprobe showed calibration equation of $y = 0.1014x - 0.0737$, $R^2 = 0.9925$. The detection limit (LOD) and the quality limit (LOQ) was 0.12 ppm and 0.38 ppm. Respectively. The analytical performance CdS-Cys-DAB nanoprobe are similar to the ICP-MS method on selenium detection but better than the AAS method.

The proposed method of measuring selenium(IV) in the vegetable sample was applied. The selenium level content in the water sample was approximate 0.2 μg and observe more in the river sample. In the vegetable sample, selenium levels were approximate 0.93 μg and more find in garlic samples. The intensity of fluorescence depends on the amount of selenium on the surface of the nanoprobe. No separation process is required in this method to reduce the background fluorescence signals. The change in intensity shed light also depends on how the fluorescent nanoprobe is designed in another sample to monitor selenium(IV).

REFERENCES

1. Clark L, Combs G, Turnbull B, Slate E. Effects of selenium supplementation for cancer prevention in patients with carcinoma of the skin. A randomized controlled trial. Nutritional Prevention of Cancer Study Group. *JAMA*. 1996;276(24):1957-63.
2. Hill K, Chittum H, Lyons P, Boeglin M, Burk R. Effect of selenium on selenoprotein P expression in cultured liver cells. *Biochimica et Biophysica Acta*. 1996;1313:29-34.
3. Lopez-Saez JB, Senra-Varela A, Pousa-Estevez L. Selenium in breast cancer. *Oncology*. 2003;64(3):227-31.
4. Shamberger RJ. *Analytical Methods of Selenium Determination*. New York and London: Plenum Press; 1983.
5. Lakowicz JR. *Principles of Fluorescence Spectroscopy*. 3 ed. New York: Springer US; 2006.
6. Liang S, Chen J, Pierce DT, Zhao JX. A turn-on fluorescent nanoprobe for selective determination of selenium(IV). *ACS Appl Mater Interfaces*. 2013;5(11):5165-73.
7. Lp C, J.Lisk D. Enrichment of selenium in allium vegetables for cancer prevention. *Cardnogeoesfs* 1994;15(9):1881-5.
8. Belman S. Onion and garlic oils inhibit tumor promotion. *Carcinogenesis*. 1983;4(8):1063-5.
9. Goldman IL, Schwartz BS, Kopelberg M. Variability in Blood Platelet Inhibitory Activity of Allium (Alliaceae) Species Accessions. *American Journal of Botany*. 1995;82(7):827-32.
10. Serlin I. Fluorometric determination of selenium in plants and animals with 3,3'-diaminobenzidine. Caution notice. *Analytical Chemistry*. 1963;35(13):2221-.
11. Soldenhoff K, inventor; Australian nuclear science and technology organisation, assignee. Selective gold extraction from copper anode slime with an alcohol. United States 2011.
12. Nancharaiah YV, Lens PN. Ecology and biotechnology of selenium-respiring bacteria. *Microbiol Mol Biol Rev*. 2015;79(1):61-80.

13. Winkel LH, Vriens B, Jones GD, Schneider LS, Pilon-Smits E, Banuelos GS. Selenium cycling across soil-plant-atmosphere interfaces: a critical review. *Nutrients*. 2015;7(6):4199-239.
14. Kesterson-Program. Final environmental impact statement: Sacramento, CA : U.S. Bureau of Reclamation; 1986.
15. Burau RG. Environmental chemistry of selenium. *California agriculture*. 1985:16-8.
16. Jezek P, Skarpa P, Losak T, Hlusek J, Juzl M, Elzner P. Selenium – An Important Antioxidant in Crops Biofortification. London: INTECH; 2012.
17. Haygarth PM, Harrison AF, Jones KC. Geographical and seasonal variation in deposition of selenium to vegetation. *Environmental science & technology*. 1993;27(13):2878.
18. Surai PF. Selenium in nutrition and health. Nottingham: Nottingham University Press 2005.
19. Eich-Greatorex S, Sogn TA, Øgaard AKF, Aasen I. Plant availability of inorganic and organic selenium fertiliser as influenced by soil organic matter content and pH. *Nutrient Cycling in Agroecosystems* 2007;79(3):221-31.
20. Shahzad SA. Novel Selenium-Mediated Rearrangements and Cyclisations. New York: Springer-Verlag Berlin Heidelberg; 2013.
21. Tinggi U. Selenium: its role as antioxidant in human health. *Environ Health Prev Med*. 2008;13(2):102-8.
22. Chen J, Zhu Y. Solid State Fermentation for Foods and Beverages. 1 ed. Florida: CRC Press; 2013.
23. Di Bella S, Grilli E, Cataldo MA, Petrosillo N. Selenium deficiency and HIV infection. *Infect Dis Rep*. 2010;2(2):e18.
24. Dan PM. Essential Oils and Healthy Menopause: History and Research Secrets. 1 ed. Vermont: DP Publishing; 2015.
25. Nordberg G, Fowler B, Nordberg M. Handbook on the Toxicology of Metals. cambridge: Academic Press; 2014.
26. Ruta DA, Haider S. Attempted murder by selenium poisoning. *BMJ*

1989;299(6694):316-7.

27. Dowling AP. Development of nanotechnologies. *Materials Today*. 2004;7(12):30-5.

28. Nagarajan R. Nanoparticles: Building Blocks for Nanotechnology. ACS Symposium Series. 2008;996:2-14.

29. Scherrer P. Nanoparticle production – How nanoparticles are made: Laboratory for Micro and Nanotechnology; [Available from:

https://www.nanowerk.com/how_nanoparticles_are_made.php.

30. Yu HD, Regulacio MD, Ye E, Han MY. Chemical routes to top-down nanofabrication. *Chem Soc Rev*. 2013;42(14):6006-18.

31. Jain P, Huang X, El-Sayed I, El-Sayed M. Noble metals on the nanoscale: optical and photothermal properties and some applications in imaging, sensing, biology, and medicine. *Accounts of Chemical Research*. 2008;41(12):1578-86.

32. Nordlander P. Applied physics. Molecular tuning of quantum plasmon resonances. *Science*. 2014;343(6178):1444-5.

33. Jamieson T, Bakhshi R, Petrova D, Pocock R, Imani M, Seifalian AM. Biological applications of quantum dots. *Biomaterials*. 2007;28(31):4717-32.

34. Abdelmonem AM. Nanoparticles: Synthesis, Surface Modification and Functionalization for Biological and Environmental Applications 1ed. Marburg Philipps-Universität Marburg 2014.

35. Shubayev VI, Pisanic TR, 2nd, Jin S. Magnetic nanoparticles for theragnostics. *Adv Drug Deliv Rev*. 2009;61(6):467-77.

36. Tang SC, Lo IM. Magnetic nanoparticles: essential factors for sustainable environmental applications. *Water Res*. 2013;47(8):2613-32.

37. Drago RS. Physical methods for chemists: Saunders College Pub; 1992.

38. Whittaker AG, Mount AR, Heal MR. Physical Chemistry: BIOS Scientific; 2000.

39. Willard H, Merritt L, Dean J. Instrumental Methods of Analysis. 5 ed: Van Nostrand; 1974.

40. Atkins P, Paula Jd. Atkins' Physical Chemistry. 8 ed. English: OUP Oxford; 2006.

41. Frackowiak D. The Jablonski diagram. *Journal of Photochemistry and Photobiology*

B: Biology. 1988;2(3):399.

42. Leach A. Molecular Modelling: Principles and Applications. 2 ed: Pearson; 2001.

43. Parr RG, Yang W. Density functional theory of Atoms and Molecules. New York: Oxford; 1989.

44. Runge E, Gross EKV. Density-Functional Theory for Time-Dependent Systems. Physical Review Letters. 1984;52(12):997-1000.

45. Zangwill A, Soven P. Density-functional approach to local-field effects in finite systems: Photoabsorption in the rare gases. Physical Review A. 1980;21:1561.

46. Walkinson JH. Fluorometric determination of selenium in biological material with 2,3-diaminonaphthalene. Analytical Chemistry. 1966;38(1):92-7.

47. Handelman G, Kosted P, Short S, Dratz E. Determination of selenium in human blood by high-performance liquid chromatography with fluorescence detection. Analytical Chemistry. 1989;61:2244-9.

48. Niedzielski P, Siepak M, Siepak J, Przybytek J. Determination of different forms of arsenic, antimony and selenium in water samples using hydride generation. Polish Journal of Environmental Studies. 2002;11(3):219-24.

49. Larsen EH, Sloth J, Hansen M, Moesgaard S. Selenium speciation and isotope composition in ⁷⁷Se-enriched yeast using gradient elution HPLC separation and ICP-dynamic reaction cell-MS. Journal of Analytical Atomic Spectrometry. 2003;18(4):310-6.

50. Stripeikis J, Tudino M, Troccoli O, Wuilloud R, Olsinab R, Martinez L. On-line copper and iron removal and selenium(VI) pre-reduction for the determination of total selenium by flow-injection hydride generation-inductively coupled plasma optical emission spectrometry. Spectrochimica Acta Part B Atomic Spectroscopy. 2001;56(1):93-100.

51. Feng G, Dai Y, Jin H, Xue P, Huan Y, Shan H, et al. A highly selective fluorescent probe for the determination of Se(IV) in multivitamin tablets. Sensors and Actuators B: Chemical. 2014;193:592-8.

52. Wang H-F, Wu S-P. Highly selective fluorescent sensors for mercury(II) ions and their applications in living cell imaging. Tetrahedron. 2013;69(8):1965-9.

53. Mansour AM. Tazarotene copper complexes: Synthesis, crystal structure, DFT and

biological activity evaluation. *Polyhedron*. 2016;109:99-106.

54. Devi RA, Latha M, Velumani S, Oza G, Reyes-Figueroa P, Rohini M, et al. Synthesis and Characterization of Cadmium Sulfide Nanoparticles by Chemical Precipitation Method. *J Nanosci Nanotechnol*. 2015;15(11):8434-9.

55. Koneswaran M, Narayanaswamy R. RETRACTED: Mercaptoacetic acid capped CdS quantum dots as fluorescence single shot probe for mercury(II). *Sensors and Actuators B: Chemical*. 2009;139(1):91-6.

56. Hoste J, Gillis J. Spectrophotometric determination of traces of selenium with diaminobenzidine. *Analytica Chimica Acta*. 1955;12:158-61.

57. Wang Y, Xia Y. Bottom-Up and Top-Down Approaches to the Synthesis of Monodispersed Spherical Colloids of Low Melting-Point Metals. *Nano Letters*. 2004;4(10):2047-50.

58. Thermofisher. EDC (1-ethyl-3-(3-dimethylaminopropyl)carbodiimide hydrochloride) [Available from: <https://www.thermofisher.com/order/catalog/product/22980#/22980>.

59. Dye WB, Bretthauer E, Seim HJ, Blincoe C. Fluorometric Determination of Selenium in Plants and Animals with 3,3'-Diaminobenzidine. *Analytical Chemistry*. 1963;55(11):1687-93.

60. Zhao D, Ma W, Wang R, Yang X, Li J, Qiu T, et al. The Preparation of Green Fluorescence-Emissioned Carbon Dots/Poly(N-Isopropylacrylamide) Temperature-Sensitive Hydrogels and Research on Their Properties. *Polymers (Basel)*. 2019;11(7).

61. Zhang Y-Y, He X-W, Li W-Y. Study on the room temperature synthesis of highly photoluminescent and temperature-sensitive CDs/PNIPAM hybrid hydrogels and their properties. *RSC Advances*. 2015;5(87):71030-4.

62. Medicine Io. Dietary Reference Intakes: Vitamin C, Vitamin E, Selenium, and Carotenoids. Washington DC: National Academy Press; 2000.

63. Agriculture USDo. Agricultural Research Service Nutrient Data Laboratory Home Page2011 [Release 24:[Available from: <https://www.ars.usda.gov/northeast-area/beltsville-md-bhnrc/beltsville-human-nutrition-research-center/methods-and-application-of-food-composition-laboratory/>].





APPENDIX

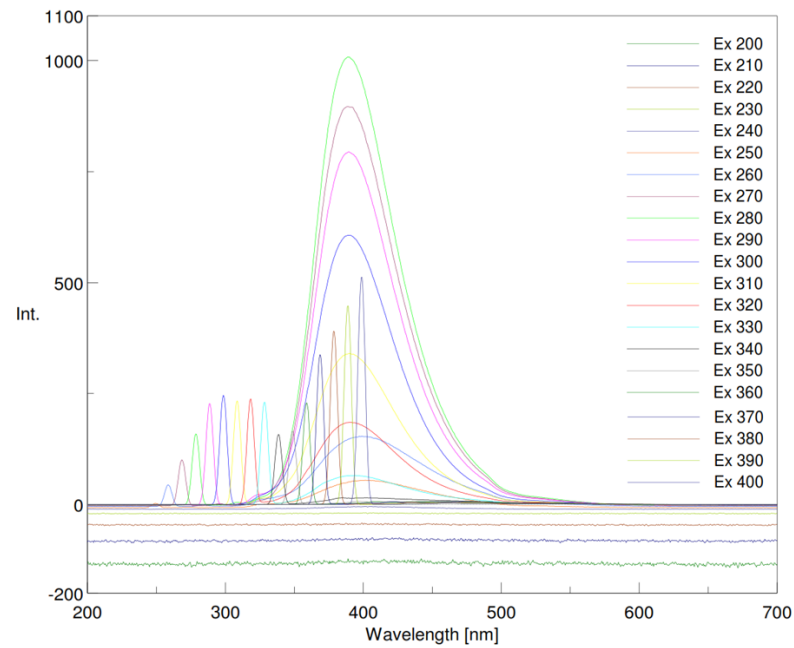


Figure 36 Spectrum of QD-DAB-Se form fluorescence spectrophotometer Model: Jasco, code FP-6200 PC (USA)

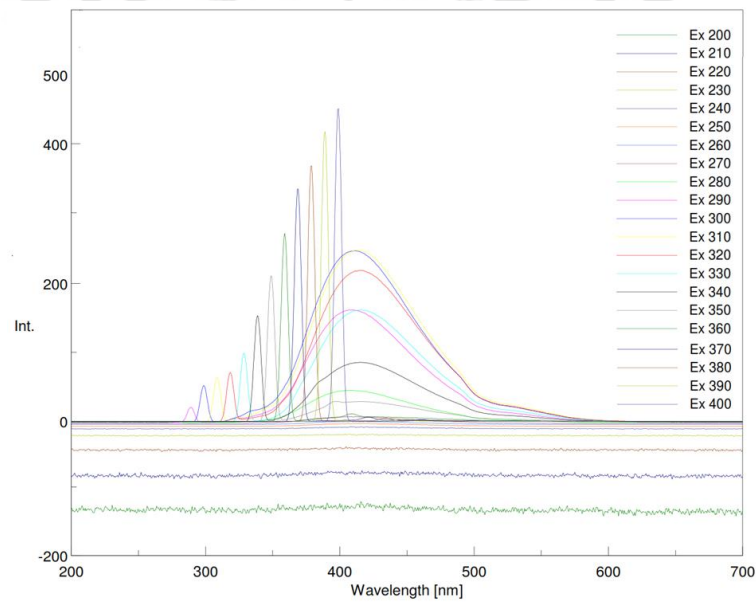


Figure 37 Spectrum of DAB-Se form fluorescence spectrophotometer Model: Jasco, code FP-6200 PC (USA)

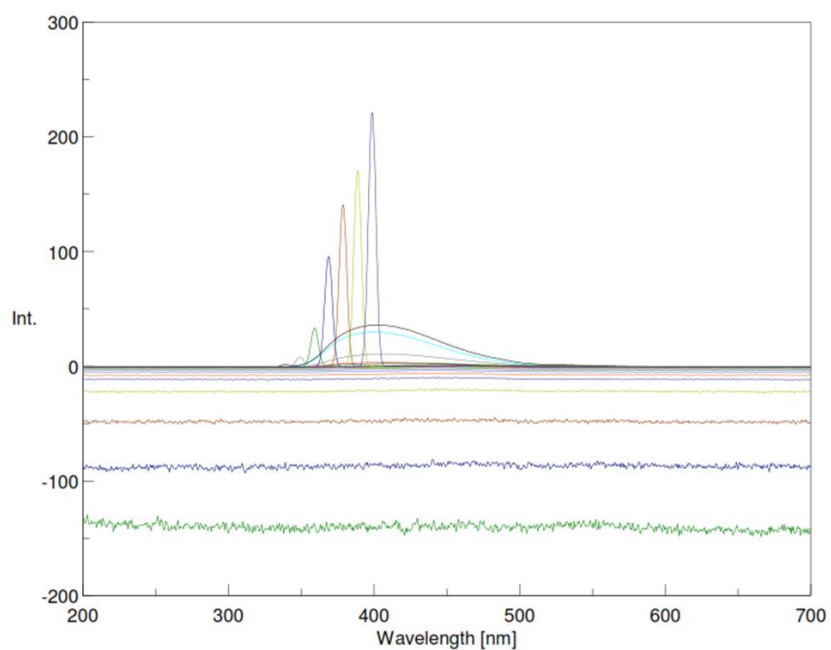


Figure 38 Spectrum of CdS-DAB form fluorescence spectrophotometer Model: Jasco, code FP-6200 PC (USA)

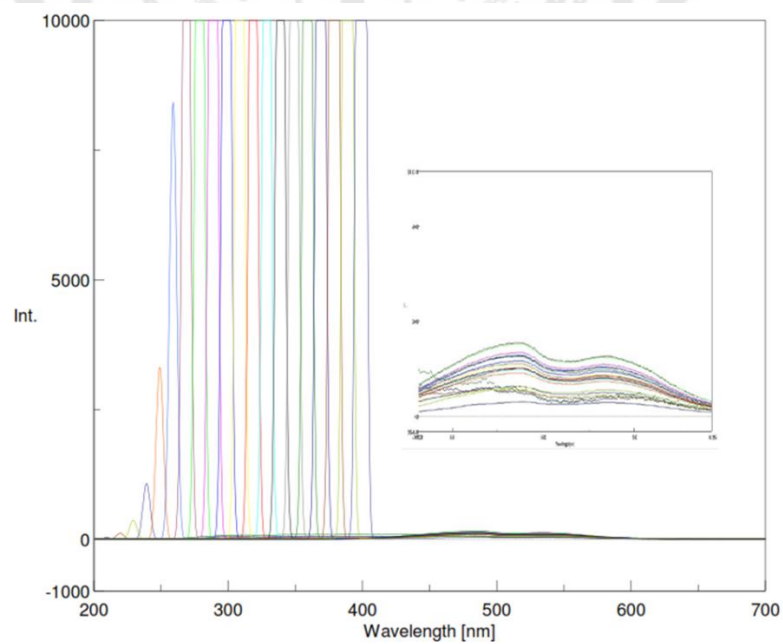


Figure 39 Spectrum of CdS form fluorescence spectrophotometer Model: Jasco, code FP-6200 PC (USA)

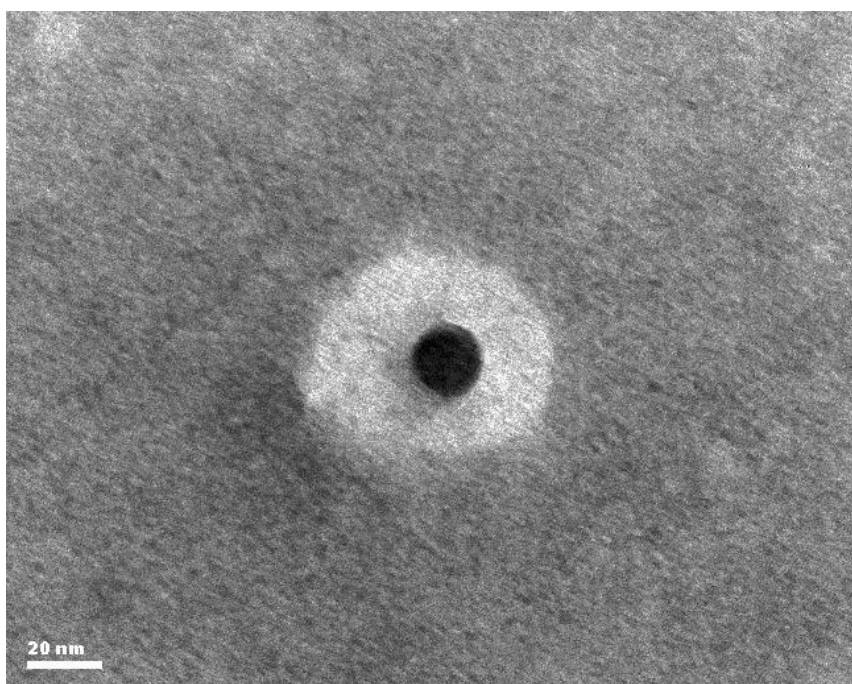


Figure 40 TEM image of CdS core particle.

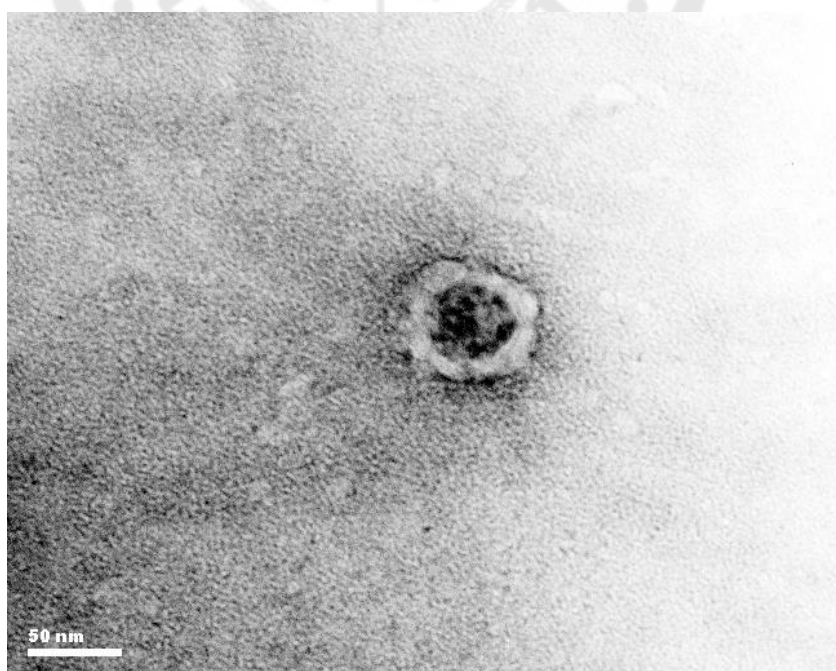


Figure 41 TEM image of CdS core particle after immobilized.

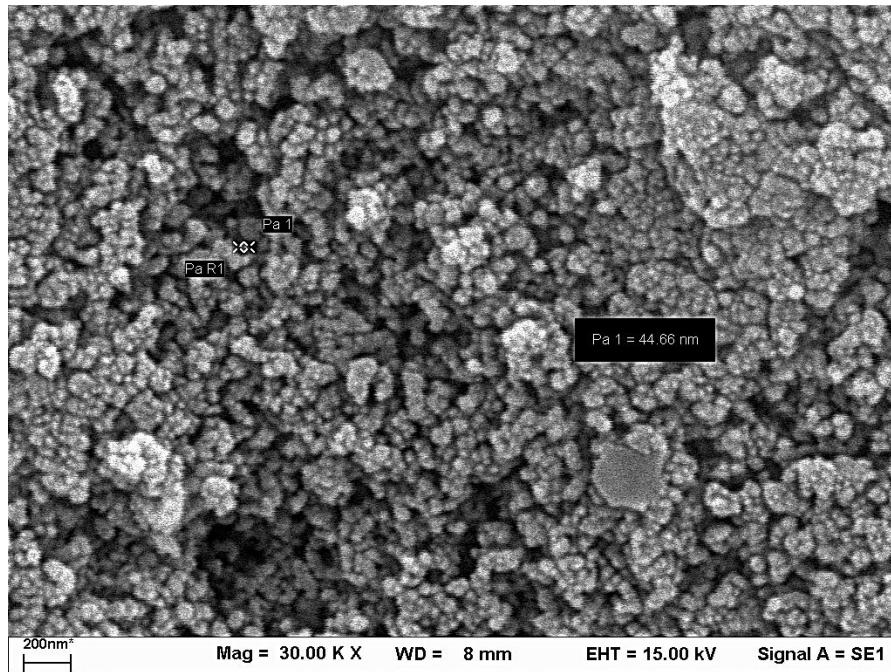


Figure 42 SEM image of CdS core particle.

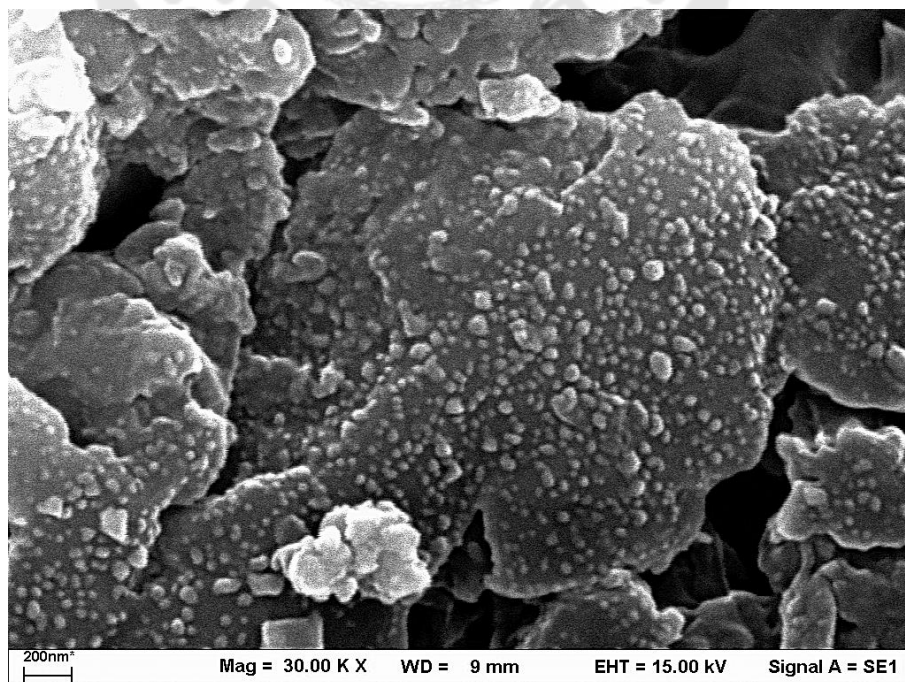


Figure 43 SEM image of CdS core particle after immobilized with DAB.



Figure 44 Setting of Synthesis of CdS-Cys-DAB nanoprobe.



Figure 45 Precipitation effect at high pH and high temperature



Figure 46 Fluorescent property in UV-lamp after synthesis finally.



Figure 47 Precipitated by addition of ethanol and solvent (water)



Figure 48 Shallot, garlic and onion sample for selenium(IV) analysis



GLOSSARY

LIST OF ABBREVIATIONS AND SYMBOLS

α	=	Alpha
AAS	=	Atomic absorption spectrometry
β	=	Beta
$^{\circ}\text{C}$	=	Degree Celsius
Conc	=	Concentration
calcd	=	Calculated
cm	=	Centimeter
cm^{-1}	=	Reciprocal centimeter (unit of wave number)
DAB	=	Diaminobenzidine
g	=	Gram
h	=	Hour
Hz	=	Hertz
IC_{50}	=	50% Inhibitory Concentration
IR	=	Infrared Spectrum
J	=	Coupling constant
Kg	=	Kilogram
L	=	Liter
λ_{max}	=	Wavelength at maximal absorption
ϵ	=	Molar absorptivity
mg	=	Milligram
m/z	=	Mass to charge ratio
mL	=	Milliliter
ppb	=	Parts per billion (ng/g)
ppm	=	Parts per million ($\mu\text{g/g}$)
μl	=	Microliter
μg	=	Microgram
nm	=	Nanometer

VITA

NAME Jaturong Chongcharoen

DATE OF BIRTH 8 December 1982

PLACE OF BIRTH Nonthaburi

INSTITUTIONS ATTENDED Bachelor's Degree, Chemistry, Srinakharinwirot university
Master's Degree, Chemistry, Srinakharinwirot university

HOME ADDRESS 60 M3, Un Suk Alley, Suan Prink Thai, Mueang Pathum Thani
District, Pathum Thani 12000

